Photochromic Sodalites by a New Method of Synthesis

Master's thesis

Teppo Kreivilä

Intelligent Materials Chemistry

Department of Chemistry

University of Turku

October 2021

Master's thesis

Subject: Chemistry
Author: Teppo Kreivilä
Title: Photochromic Sodalites by a New Method of Synthesis
Supervisors: Mika Lastusaari, Hannah Byron, Sami Vuori and Isabella Norrbo
Number of pages: 37
Date: October 2021

Photochromic sodalites, also known as hackmanites, are minerals that belong to the sodalite mineral group and have a general formula of $Na_8(SiAlO_4)_6(Cl,S)_2$. Hackmanites can exhibit reversible photochromism i.e., tenebrescence, photoluminescence and persistent luminescence upon UV irradiation. In tenebrescence, hackmanite changes colour, traditionally from white to purple corresponding to a formation of an F-centre which absorbs light of around 540 nm, after UV or X-ray irradiation. The tenebrescence colour can be bleached with either heat or visible light.

Synthesized hackmanites show various luminescence and tenebrescence properties, and, for the first time, yellow and near-infrared tenebrescence are reported for hackmanites. Hackmanites with these exciting new properties could potentially be used as materials for different applications, including advanced anti-counterfeiting.

Keywords: hackmanite, luminescence, tenebrescence, photochromism

Table of Contents

Abbreviations

c-Si = Crystalline silicon

EPR = Electron paramagnetic resonance

EVA = Ethylene vinyl acetate

ICP-MS = Inductively coupled plasma mass spectrometry

LDS = Luminescent down shifting

PeL = Persistent luminescence

PMMA = Polymethyl methacrylate

TL = Thermoluminescence

UC-PL = Up-conversion photoluminescence

XPS = X-ray photoelectron spectroscopy

XRD = X-ray powder diffraction

XRF = X-ray fluorescence spectroscopy

1 Introduction

Already discovered in 1930s[1], sodalites are minerals that belong to sodalite mineral group and have a general formula of $Na_8(SiAlO_4)_6Cl_2$..[2] Sodalites have been found from nature, for instance, from Canada, Afghanistan and Pakistan[3] but they can also be produced synthetically. Once sodalites are synthesized with the addition of a sulphur source, they can show reversible photochromism, also known as tenebrescence[4]. These materials are called photochromic sodalites or hackmanites, have a general formula of $Na_8(SiAlO_4)_6(Cl,S)_2$ and can change colour upon UV-excitation.[2,4] However, hackmanite is no longer accepted as an official mineral name by International Mineralogical Association[5] advising photochromic sodalite to be the official name. Since the name hackmanite has been widely used in previous publications it will be used in this thesis as well. In addition to reversible photochromism, synthetic hackmanites are also known to have additional properties like photoluminescence and white, long-lasting persistent luminescence (PeL)[6,7]. Synthetically produced hackmanites do not contain environmentally toxic heavy metals nor expensive lanthanides[6], which makes them relatively inexpensive to produce. In addition, hackmanites can be tailored to show different luminescence colours and lifetimes.[6] All things considered, hackmanites could be potentially used in different applications as optical and diagnostic markers[6,7] or in UV dosimetry[8].

1.1 The structure of sodalite

The understanding of the sodalite structure (**Figure 1**) is important, since the mechanisms of photochromism and PeL can be explained by structural changes in the sodalite structure.[9] The crystal structure of hackmanite is cubic with a space group $P\bar{4}3n$ with a unit-cell parameter equal to 8.88696(5) Å.[10] The sodalite β-cage framework is formed by vertex linkage of SiO_4^{4-} and AlO_4^{5-} tetrahedra forming either six-rings or

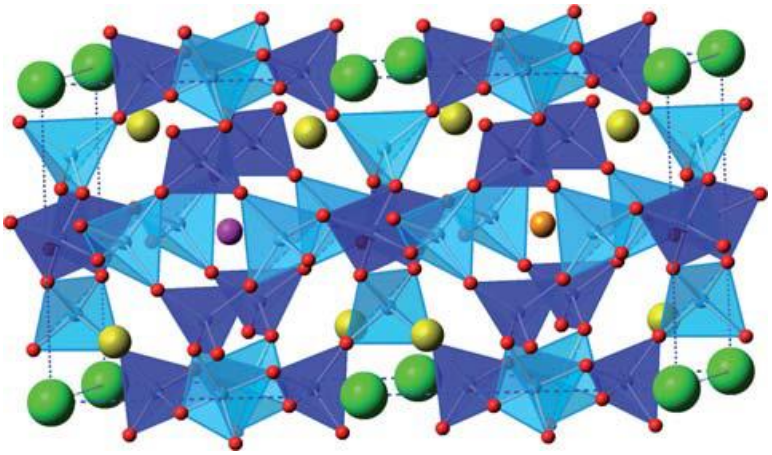

Figure 1. Sodalite structure. Dark blue tetrahedra represent SiO_4^{4-}, light blue tetrahedra represent AlO_4^{5-} and yellow, green and red balls represent sodium ions, chloride ions and oxide ions, respectively. The purple ball represents a sulphur-ion and the orange ball represents the chlorine vacancy. (Reproduced from Williams et al.[13] with permission from the Royal Society of Chemistry)

four-rings between the cages with an ordered distribution of Al and Si atoms. The β-cage has cavities, which contain large anions like Cl^- ions, which are tetrahedrally coordinated by four Na atoms together forming $(Na_4Cl)^{3+}$ entities. The Na atoms in these entities are fourfold coordinate by one Cl^- ion and three framework O^{2-} ions.[10,11] In hackmanite, some of the Cl^- ions have been substituted by sulphur-containing ions like SO_4^{2-}, S^{2-}, S_2^{2-} or S_3^{2-}. When the sodalite structure is irradiated, for example, with UV radiation, an electron is excited from an electron-rich sulphur species in one sodalite cage and becomes trapped in a chlorine vacancy in a nearby cage. This causes the forming of an F-centre[12], which causes photochromism in sodalites.[13]

The mineral composition has an important effect on sodalite's spectroscopic properties.[6,14] Zahoransky et al.[14] investigated natural sodalites and found out that sodalites with a lower sulphur concentration have a smaller unit-cell parameter *a,* which also showed that the sodalite samples showing strong tenebrescence have a smaller unit-cell compared to the sodalite samples showing weaker tenebrescence. The same observation has also been made for synthetic sodalites.[6] Sodalites must contain sulphur to achieve tenebrescence, however, too high a concentration of sulphur leads to the saturation of tenebrescence and no colour change is obtained. This also applies to photoluminescence in sodalites: higher concentrations of sulphur lead to stronger photoluminescence, but too high concentrations result in self-quenching.[14] Zahoransky et al.[14] suggested that the lack of tenebrescence in sodalite samples containing high concentrations of sulphur is due to the changes in the sodalite structure, which interrupts the formation of F-centres. Additionally, the Si:Al ratio of synthetic sodalites should be kept as close to 1:1 to achieve the strongest tenebrescence, since changes in this ratio may cause disruptions in the atomic or electronic structure of the synthetic sodalite.[15]

1.2 The luminescence properties of natural and synthetic hackmanites

Luminescence-wise, natural and synthetic sodalites have similarities although synthetic sodalites can emit different colours upon doping[16]. The emission colour of natural hackmanites have been investigated by Agamah et al.[3] and depends highly on the excitation wavelength and the origin of the sample. With excitation at 355 nm, natural hackmanites show orange emission peaking at around 615 nm and with excitation at 295 nm a green/blue emission peak at around 500 nm appears in addition to an emission peak at 615 nm. Additionally, a red emission peak at around 720 nm can also sometimes be seen when excited with 295 nm. Emission peaks at similar wavelengths can also be found

with excitation at 255 nm. The orange emission at around 615 nm originates from the S_2^- luminescence centre[17] and the green/blue emission at around 500 nm is assigned to the Ti^{3+}–V_0 pair[9]. Furthermore, the red emission peak at around 720 nm can originate from either Cr^{3+} or Fe^{3+} substituting for Al^{3+} in tetrahedral sites[18]. Agamah et al.[3] concluded that it was common for natural hackmanite samples to have Fe present in all of them leading to a suggestion that the red emission in natural hackmanites originates from Fe^{3+} luminescence centres. Additionally, Agamah et al.[3] used cathodoluminescence to obtain a strong UV/blue emission peak at 350 nm, which they assigned to an F^+ centre, which is an oxygen vacancy with one electron in the vicinity of Al^{3+}.

The emission colour of synthesized hackmanites depends on the elemental composition of the sample. Agamah et al.[3] managed to synthesize a hackmanite with similar luminescence properties to natural hackmanites having emission peaks at 615 nm and 500 nm with excitation at 355 nm, and 295 nm and 254 nm, respectively. Furthermore, Norrbo et al.[6] synthesized a non-doped hackmanite with an emission peak at 460 nm, which was later assigned to originate from the Ti^{3+}–V_0 pair[9]. Partly replacing Na ions with Li ions made the emission peak more intense and gave a bright PeL emission peaking at 500 nm.[7] Additionally, green emission at 540 nm originating from Mn^{2+} luminescence centres have also been reported for synthetic sodalites, in addition to blue emission at 450 nm originating from O_2^- entities.[19] Finally, Byron et al.[20] prepared hackmanites with a zeolite-free synthesis, which resulted in a hackmanite with an emission peak at 460 nm.

Synthetic sodalites can be tuned, for example, by changing the amounts of starting reagents in the synthesis, by replacing sodium cations with other cations, for example potassium, calcium or strontium, or doping with different ions.[6,7,20] This can improve the properties of synthetic sodalites. Hackmanites, synthesized with different S:Cl ratios, showed various emission colours when excited with different UV wavelengths and, additionally, intensities of tenebrescence varied with different S:Cl ratios, suggesting that the strongest tenebrescence colour would be gained when the S:Cl ratio is close to 0.06.[6] In addition, Norrbo et al.[7] managed to obtain record-long duration of white PeL without the use of rare earths by partly replacing sodium cations with lithium cations and upon 2 % Ti^{3+} doping. Byron et al.[20] also mentioned that hackmanites could be more finely tuned when using a zeolite-free synthesis method to produce them since

the amounts of aluminium, silicon and sodium could be individually alternated in the synthesis.

1.3 Suggested mechanisms of tenebrescence

Reversible photochromism, i.e., tenebrescence, is a reversible process, where material can change colour upon excitation with, for instance, UV radiation or X-rays. The decolouration of the material can then be induced by light or heat.[4] In addition to mechanism of PeL, Norrbo et al.[9] put forward the mechanism of tenebrescence in synthetic hackmanite. Before their research, the tenebrescence of hackmanites was known to arise from chlorine vacancies that capture electrons originating from electron-rich sulphur-ions after irradiation with UV radiation.[4] Electrons get trapped in chlorine vacancies and form colour centres, i.e., F-centres, which cause the photochromism of the material.[2,4,13] Norrbo et al.[9] performed tenebrescence excitation measurements and concluded that the sulphur source is S_2^{2-} ion with a ground level of the ion located 4.3 eV below the bottom of the conduction band. Next, they measured colour bleaching spectra, which showed that the ground level of the colour centre was located 2.0 eV below the conduction band. Electron paramagnetic resonance (EPR) measurements also indicated that tenebrescence and PeL take place in different parts of the hackmanite structure. Finally, Norrbo et al.[9] presented the mechanism of tenebrescence in synthetic hackmanites as seen in (**Figure 2**): Tenebrescence occurs in $Na_4(□,S)$ entities (□ represents a vacancy on the anion site, usually a chlorine vacancy). S_2^{2-} ion absorbs energies 4.3 eV and above and transfers electrons from its excited levels to the conduction band in the charging stage. After that, the F-centres are formed in the chloride vacancies where electrons have transferred via the conduction band. F-centres absorb visible light between 1.8 and 2.9 eV resulting in the purple colour of hackmanite. Finally, in the decharging stage, the absorbed light gradually lifts electrons back to the excited levels of the S_2^{2-} ion and the decolouration of hackmanite occurs.

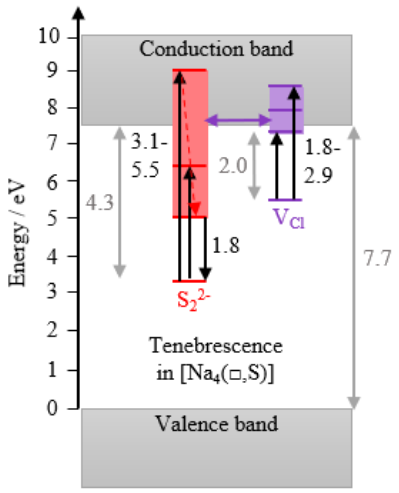

Figure 2. Two-step mechanism of tenebrescence in synthetic hackmanites as presented first by Norrbo et al.[9].

Although this mechanism seems possible, Curutchet and Le Bahers[21] calculated the transition energy between the highest occupied crystalline molecular

orbital localized on the disulphide and the conductive band of sodalite to be around 7 eV, which is higher than the one used to generate the F-centre proposed by Norrbo et al.[9], thus, making the proposed mechanism less attractive. However, Curutchet and Le Bahers[21] pointed out that a deeper quantum chemical investigation of the mechanism proposed by Norrbo et al.[9] is necessary before ruling it out. Another mechanism of tenebrescence was later proposed by Norrbo et al.[8], which shows that, at first, a photon-induced electron transfer happens between S_2^{2-} and V_{Cl}. Then, a geometrical relaxation induces an electronic state reorganization, which brings the system to a stable triplet state of one unpaired electron on both S_2^- and V_{Cl}. The coloration of the system is due to allowed electronic transition $^3[S_2^-, V_{Cl}^- (t_2)] \leftarrow {}^3[S_2^-, V_{Cl}^- (a_1)]$ and the bleaching of the system is associated with populating of the $^1[S_2^{2-}, V_{Cl}]$ state.

1.4 Materials developed for anti-counterfeiting applications

With globalization and international trade developing rapidly, counterfeiting has become problematic and causes economic losses, while also potentially causing health issues with food and medicine also being counterfeited. For that reason, simple anti-counterfeiting technologies have been developed, like watermarks and holograms, however, these are easy to imitate. Therefore, functional materials with unique, unclonable properties based on, for example, luminescence and photochromism need to be developed.[22]

Materials developed for anti-counterfeiting applications can be both inorganic and organic.[22,23] To name a few, Wang et al.[22] presented D–A type inverse diarylethene, which undergoes isomerization and shows green emission upon 365 nm UV irradiation in CH_2Cl_2 solution. The green emission vanishes instantly once irradiation is stopped making it a potential application for anti-counterfeiting materials. Additionally, another anti-counterfeiting application based on reversible photochromism of $BaMgSiO_4:Yb^{3+},Tb^{3+}$ ceramic was presented by Ren et al.[23]. The ceramic exhibited reversible photochromism from gray to pink after 254 nm UV irradiation. Furthermore, the pink colour could be bleached with a 473 nm laser or thermal stimulation, and they were able to repeat the reversible process after several cycles, making it possible material to be used in anti-counterfeiting applications.

In addition to materials showing one property suitable for anti-counterfeiting applications, several materials have been developed that show multiple properties suitable for anti-counterfeiting applications providing possibilities for multimode advanced anti-counterfeiting.[24–26] For instance, Huang et al.[24] synthesized a

novel tetraphenyl ethylene showing different luminescence properties in tetrahydrofuran and water, mechanochromism properties when ground and fumed in dichloromethane and red photochromism under 365 nm UV irradiation due to an increase in conjugation of the molecules. The luminescent behaviour coming from mechanochromism can be bleached by heating the powder to 120 °C, while the red photochromism faded away 60 s after the initial UV irradiation making this material suitable for multidimensional anti-counterfeiting applications. Additionally, Xu et al.[26] proposed $CsPbBr_3/Cs_4PbBr_6$ perovskite nanocrystals dispersed in silica gel showing green photoluminescence emission under 325 nm UV irradiation and green up-conversion photoluminescence (UC-PL) emission under 800 nm NIR laser, while also showing temperature-dependent green emission when heated between 25–150 °C, the emission of the material becoming weaker at higher temperatures. Consequently, this triple-mode emission is suitable for anti-counterfeiting applications. Finally, Jiang et al[25] synthesized carbon dots also capable of triple-mode emission showing blue photoluminescence emission under 365 nm UV irradiation, cyan UC-PL emission under 800 nm NIR laser and green PeL after 365 nm UV irradiation. These carbon dots can be incorporated in polyvinyl alcohol matrix providing a luminescent ink, capable to be applied in anti-counterfeiting applications.

1.5 The background and goal of this work

Several methods have been used previously to synthesize sodalites: a solid-state synthesis[6], a hydrothermal synthesis[27] and a microwave-assisted synthesis[28]. In addition, Norrbo et al.[6] used zeolite A as a starting reagent in the solid-state synthesis of hackmanites while Byron et al.[20] synthesized hackmanites with a zeolite-free method using Al_2O_3, SiO_2 and Na_2CO_3 or NaOH as starting materials instead of zeolite. Additionally, ion-exchange syntheses will be performed to obtain additional starting reagents by cation-exchange of sodium with potassium and calcium, respectively. Yang et al.[29] managed to convert calcined zeolite beta powders into alkali and alkaline earth metal ion-exchanged forms and this method will be referred to as the "solution method". Furthermore, Kayiran et al.[30] managed to fully ion exchange Na A zeolites with potassium and lithium with a simple synthesis taking place in a drying oven. Thus, this method will be referred to as the "drying oven method". Finally, a solid-state synthesis between zeolite A and different fluorides will also be investigated in this work.

The goal of this work is to successfully synthesize hackmanites using various starting reagents. This may increase the unit-cell size of the hackmanite sample.

Additionally, various cations and anions will be tried to get inside the sodalite structure by partly replacing sodium cations and chlorine anions with them. Incorporation of new anions and cations in addition to using new starting materials in the synthesis may produce new properties in hackmanites, including different photoluminescence colours and colour intensities, different PeL colours and durations or new tenebrescence colours. Indeed, a new yellow colour of tenebrescence for hackmanites will be presented in this thesis, which was obtained by partly exchanging sodium ions with calcium ions.

2 Experimental

2.1 Materials preparation

This part is not shown due to non-disclosure obligations.

2.2 Ion-exchange syntheses

In order to create additional starting reagents for further experiments, ion-exchange syntheses with three different methods were performed.

2.2.1 Solution method

At first, 1 g of zeolite A was weighted and placed in a 250 ml boiling flask. After that, 100 ml of either 1 M potassium chloride or 1 M calcium chloride was added to the flask, depending on which ion exchange was being performed. The solution was stirred and heated for 24 hours using a water-cooling system while the temperature was kept between 80–100 °C. After the heating, the solution was filtered, and the sample was washed with distilled water. Lastly, the sample was dried in a 60 °C drying oven overnight.

2.2.2 Drying oven method

To begin with, 1 g of zeolite A was weighted and placed in an Erlenmeyer flask. The K/Na ratio was kept at 13, the same ratio as Kayiran et al.[30] used in their work, by adding 92 ml of 1 M potassium chloride solution to flasks containing zeolite A. The pH of the solution was set to 9 with 0.1 M potassium hydroxide solution. Then, the solution was stirred thoroughly and placed in an 80 °C drying oven for two hours. Finally, the solution was filtered, the sample was washed with distilled water and dried in a 60 °C drying oven overnight. This procedure was carried out three times.

2.2.3 Solid-state method

At first, 0.7 g of zeolite A and a stoichiometric amount of either KF or CaF_2 were mixed and ground together by hand. Then, the mixture was placed in an aluminium oxide boat and heated in an 850 °C furnace for 5 h. After the heating, the mixture was left in room

temperature to cool down freely and ground by hand. After that, the mixture was washed with distilled water to remove excess amounts of fluorides. The amounts of fluorides used can be found in **Table S 7** in Supporting Information**.**

2.3 Tape casting

Yellow tenebrescence reversibility was investigated from sample surfaces prepared with tape casting[31]. 0.5 g of sample was poured into a 45 ml mill cup and ground in a ball mill for 10 minutes at speed 1 (400 rpm motor speed, 170 rpm ball speed). Next, 20 droplets of ethanol (approximately 0.2 g), 33 droplets of 2-butanone (approximately 0.4 g) and a droplet of triton X-100 (approximately 0.025 g) were added to the mill cup and the mixture was ground in a ball mill for 10 minutes at speed 1. After that, 3 droplets of benzyl butyl phthalate (approximately 0.08 g) and 0.09 g of polyvinyl butyral were added to the mill cup and the mixture was ground in a ball mill for 2 minutes at speed 5 (1730 rpm motor speed, 740 rpm ball speed). Finally, the suspension was placed onto a transparency and cast with the doctor blading device with a movement of ca. 5 cm s^{-1} and thickness of 200 µm. Half of the cast sample was irradiated with 254 nm UV to see the colour difference and the sample was left under daylight for three days.

2.4 Characterization methods

Structure and purity of the hackmanite samples and the ion-exchanged products were investigated using X-ray powder diffraction (XRD) measured with a Huber G670 detector and copper $K_{\alpha 1}$ radiation (λ = 1.54060 Å). Exposure time was set at 20 min and the imaging plate was read 10 times. Additionally, the unit-cell volumes of the hackmanite samples were determined with Rietveld refinements[32] using FullProf Suite's WinPlotr program. The elemental structure of the hackmanite samples and the ion-exchanged products were assessed with XRF using PANalytical Epsilon 1 device's Na 1 h program. The results are presented in weight%.

The luminescence properties of the hackmanite samples were assessed by measuring samples' photoluminescence spectra using a Varian Cary Eclipse Fluorescence Spectrophotometer containing a Hamamatsu R928 photomultiplier with a delay of 0.1 ms, a gate time of 5 ms, excitation slit 10 nm and emission slit 2.5 nm. For most measurements, the detector voltage was set at high (800 V). The PeL spectra of the samples were also measured with the same fluorescence spectrometer, however, emission slit was set at 20 nm and the sample was irradiated with a 254 nm hand-held UVLS-24 EL 4 W UV lamp for 5 minutes, followed by a 30 s delay before measurement.

The optical energy storage properties of the hackmanite samples were assessed using thermoluminescence measurements with a MikroLab Thermoluminescent Materials Laboratory Reader RA'04. Samples were irradiated with 254 nm UV from the previously mentioned lamp for 5 minutes and the thermoluminescence measurement carried out using a heating rate of 10 °C s^{-1} after a 1 min delay. Additionally, if any deep traps existed, they were assessed using preheated measurements, in which samples were preheated to 220 °C after the initial 5 min excitation and thermoluminescence measured 1 min after excitation ceased.

The photochromism properties of the hackmanite samples were investigated using reflectance measurements to investigate the F-centre's absorption band. Reflectance measurements were carried out using Avantes SensLine AvaSpec-HS-TEC spectrometer connected to an optical fibre. The reflectance of the samples before UV excitation were measured and used as a white background colour, the samples were excited with 254 nm UV from the previously mentioned lamp or with 302 nm UV from a UVP model UVM-57 6 W UV lamp for 5 minutes and their reflectance measured again 10 s after irradiation to show change in reflectance. Additionally, tenebrescence excitation measurements were carried out to find out tenebrescence intensity using different excitation wavelengths and tenebrescence colour rise curve was assessed to see how UV dosing affected the tenebrescence colour. Tenebrescence excitation measurements were assessed using Avantes SensLine AvaSpec-HS-TEC spectrometer connected with an optical fibre and LOT-QuantumDesign MSH300 monochromator and LOT-QuantumDesign LSB522 150 W xenon lamp by measuring reflectance from 200 nm to 300 nm between every 20 nm and from 300 nm to 450 nm between every 25 nm and calculating integrals between 380–580 nm for every excitation wavelength. Tenebrescence colour rise curves were measured using the same setup used in tenebrescence excitation measurements by irradiating sample with 254 nm UV from the previously mentioned lamp and measuring reflectance values every 4 s for 10 minutes. White background reference was measured 10 s after the beginning of the irradiation to take account the blue light coming from the UV excitation. Then, the integrals between 380–580 nm for every 4 s were calculated. Finally, the tenebrescence colour was further investigated by measuring CIE *L*a*b* colour coordinates with a Konica Minolta CM-2300d spectrophotometer after 5-minute 254 nm UV excitation from the previously mentioned lamp.

3 Results

The most important graphs and spectra and the results obtained from them are presented briefly in this section. The results are then more thoroughly discussed in the following Discussion section.

3.1 Different cation combinations

This chapter is divided into two sections: in the first one, all samples are synthesized using only one type of chloride and in the second one, a mixture of chlorides is used in the synthesizing of samples. The types and amounts of chlorides used can be found in **Table S 7** in the Supporting Information.

As expected, the sample made from sodium chloride has a sodalite structure with only one impurity peak at 29.4°. However, the samples made from other chlorides do not have a proper sodalite structure, with only samples made from lithium and calcium chloride showing some likeness to a sodalite structure (**Figure 3A**). The Li sample has the strongest luminescence emission under 254 nm UV irradiation having a peak at 450 nm, which is in agreement with the literature that Li enhances luminescence[7]. Additionally, the Ca sample has two luminescence emission peaks under 254 nm UV irradiation at 415 nm and 580 nm, the latter being also visible, although weaker, under 302 nm UV irradiation (**Figure 3B**). The blue emission of the Li sample can also be seen well in **Figure 3F**. Similar to emission spectra, Li sample also has the strongest PeL peak at 460 nm and Ca sample has two PeL peaks at 415 nm and 575 nm (**Figure 3C**). From these samples, only Na sample showed tenebrescence in the reflectance measurements (**Figure 3D**).

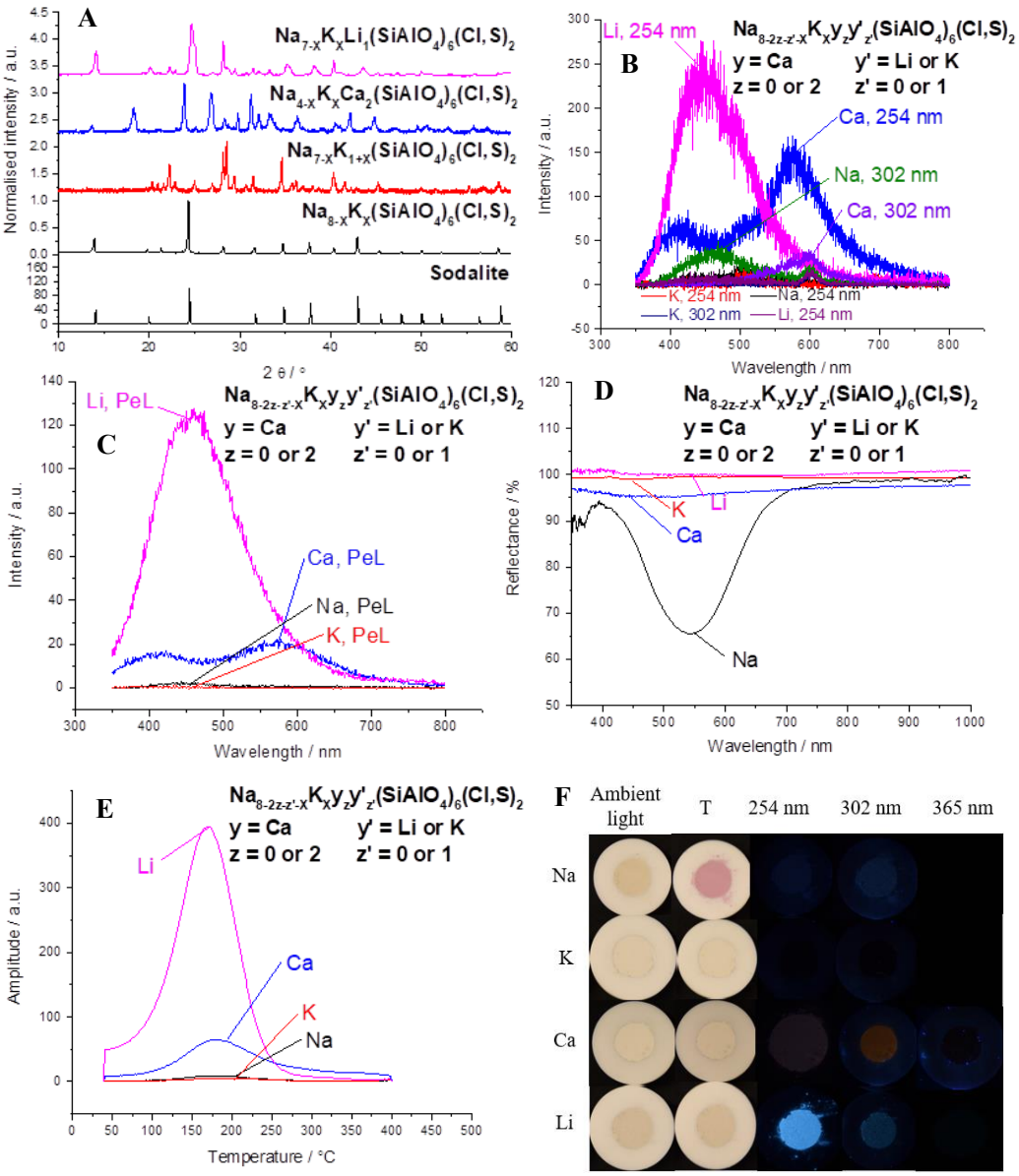

Figure 3. XRD graphs (**A**), emission spectra (**B**), PeL spectra (**C**), reflectance spectra (**D**), TL glow curves (**E**) and photographs taken under different conditions (T = tenebrescence) (**F**) of samples made using different chlorides. PeL, reflectance and TL were measured with an irradiation time and wavelength of 5 min and 254 nm, respectively.

All samples made from different ratios of chlorides have a sodalite structure, although some of the samples have less impurities than others. Both K and Ca samples have impurity peaks at 28.4° and Li and Rb samples have impurity peaks at 28.1°. Mg, Sr and Ba samples have more impurity peaks, mainly between 22.0°–30.5°. Mg sample has impurity peaks at 20.9°, 22.9°, 27.0°, 28.2° and 29.4°. Sr sample has impurity

peaks at 20.9°, 22.9°, 27.0°, 28.2°, 29.4° and 30.5°. Ba sample has impurity peaks at 22.2°, 26.4°, 27.0°, 28.1°, 29.4°, 29.9° and 39.7° (**Figure 4A**).

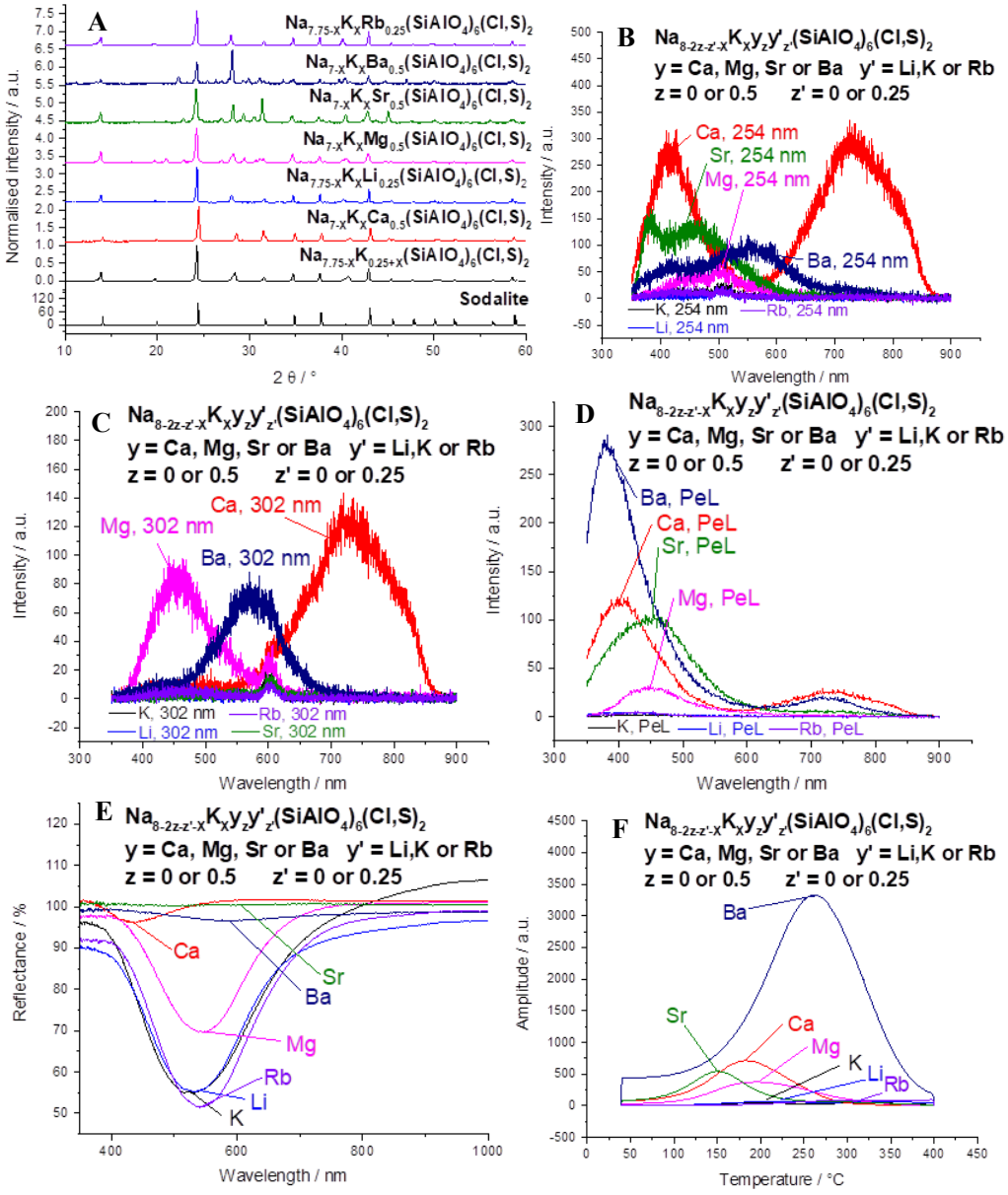

Figure 4. XRD graphs (**A**), emission spectra under 254 nm UV irradiation (**B**) and under 302 nm UV irradiation (**C**), PeL spectra (**D**), reflectance spectra (**E**) and TL glow curves (**F**) of samples made using different ratios of chlorides. PeL, reflectance and TL were measured with an irradiation time and wavelength of 5 min and 254 nm, respectively.

At 254 nm UV irradiation, Ca, Sr and Ba samples have luminescence emission peaks at 415 nm and 735 nm, 385 nm and 465 nm and 560 nm, respectively, while emission peaks for Ca, Mg and Ba samples while irradiating with 302 nm UV irradiation can be seen at 735 nm, 455 nm and 575 nm, respectively (**Figure 4BC**). Different colours of emission can also be seen at **Figure 5**. Ca, Mg, Sr and Ba samples also show PeL having PeL peaks at 405 nm, 450 nm, 455 nm and 380 nm, respectively. Additionally, Ca and Ba samples have additional PeL peaks in the NIR region (**Figure 4D**). K, Li, Mg and Rb samples have the typical, purple-coloured tenebrescence of hackmanites and have F-centre absorption bands centring at 530 nm, 530 nm, 540 nm and 540 nm, respectively. Interestingly, Ca samples has yellow tenebrescence with absorption centring at 435 nm (**Figure 4E**).

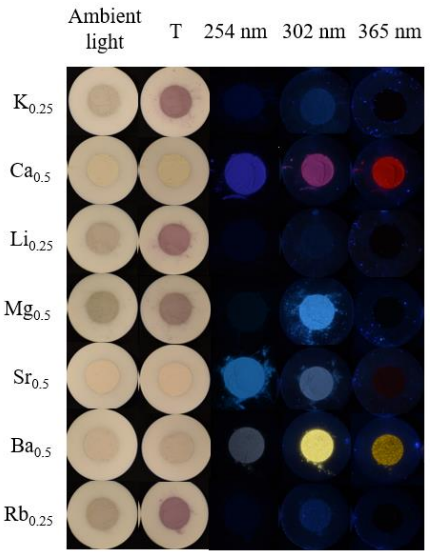

Figure 5. Photographs taken under different conditions of samples made using different ratios of chlorides (T = tenebrescence).

3.2 Different calcium salts

With the addition of calcium leading to interesting properties of yellow tenebrescence and different luminescence emission wavelengths, various calcium salts were tested next as starting materials. These salts included calcium bromide, calcium iodide, calcium carbonate, calcium phosphate and calcium fluoride.

XRD results show that only samples made with bromide and iodide have some likeness to a sodalite structure. The peaks are little shifted to the left compared to the sodalite reference. The iodide sample has impurity peaks at 21.0°, 22.8°, 27.0°, 29.4°, 30.7°, 32.4° and 32.9° while the bromide sample has impurity peaks at 26.7°, 29.0°, 32.3° and 32.9° **(Figure 6A**).

The Br sample has bright blue emission under 254 nm UV irradiation, with a peak at 410 nm. Unlike with other samples, a medium voltage detector had to be used to measure the emission and PeL, since the emission was so intense. Additionally, the CO_3 and I samples have luminescence emission peaks at 580 nm (**Figure 6B**). These emission colours are also visible in **Figure 6F**. Both Br and PO_4 samples have PeL peaks at 400 nm and a weaker peak at 735 nm (**Figure 6C**). Once more, the Br sample's PeL had to be measured using medium voltage detector. The effect of this intense PeL can

also be seen in TL glow curves, where Br sample has a peak of a very high amplitude (**Figure 6E**). Br and I samples have noticeable tenebrescence, the former having an F-centre absorption band centred at 615 nm. The latter seems to have even two F-centre absorption bands close to each other: one centred at 510 nm and second centred at 565 nm. Additionally, PO_4 sample has an F-centre absorption band centred at 600 nm (**Figure 6D**).

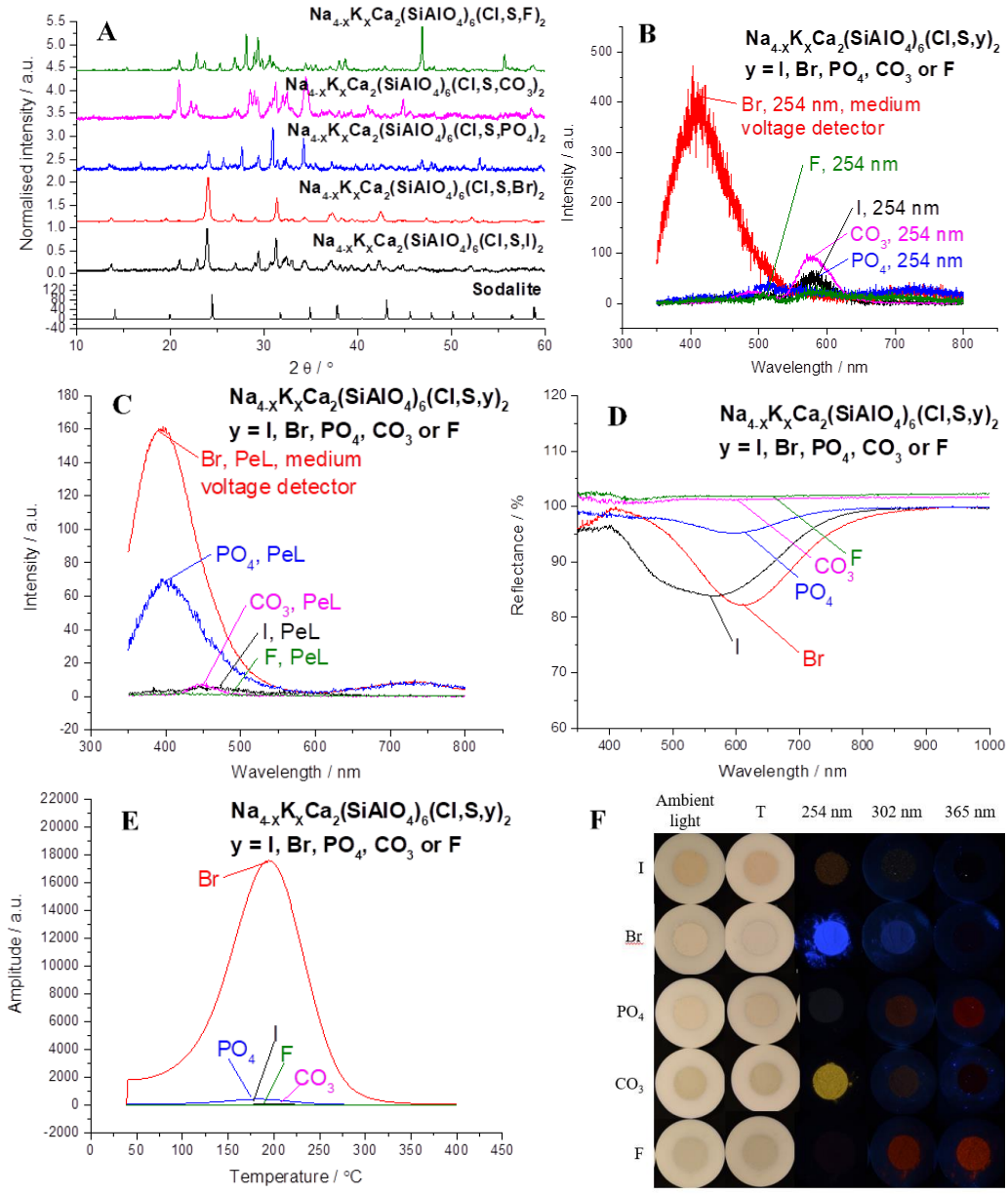

Figure 6. XRD graphs (**A**), emission spectra (**B**), PeL spectra (**C**), reflectance spectra (**D**), TL glow curves (**E**) and photographs taken under different conditions (T = tenebrescence) (**F**) of samples made using different calcium salts. PeL, reflectance and TL were measured with an irradiation time and wavelength of 5 min and 254 nm, respectively.

3.3 Ca-exchanged samples showing yellow tenebrescence

It was noticed earlier that some samples had yellow tenebrescence. This was a novel discovery, so it was investigated further by using various amounts of calcium chloride as starting material.

As explained in chapter 3.1, $Ca_{0.5}$ sample has a sodalite structure with an impurity peak at 28.4°. Likewise, other samples showing yellow tenebrescence have sodalite structures and impurity peaks at 21.0°, 22.9°, 27.0°, 28.4°, 29.4° and 40.7°. (**Figure 8A**). When irradiated with 254 nm UV, samples have luminescence emission peaks at 415 nm and 735 nm, $Ca_{0.5}$ sample having the most intense emission peaks (**Figure 8B**). When the irradiation wavelength is switched to 302 nm, the only emission peak that remains is the peak at 735 nm (**Figure 8C**). To the human eye, emission at 302 nm is purple, a mix of red and blue emission for $Ca_{0.5}$ while for other samples that emission is red to the human eye. Furthermore, emission at 254 nm is blue for all samples and at 365 nm emission is red for all samples (**Figure 7**). All samples have PeL peaks at 405 nm, $Ca_{0.5}$ sample having the most intense PeL peak. Additionally, $Ca_{0.5}$ sample has a PeL peak at NIR area (**Figure 8D**). The most interesting aspect of these samples is that they show yellow tenebrescence with F-centre absorption bands centring at 435 nm (**Figure 8E**). This yellow tenebrescence is also visible in **Figure 7**.

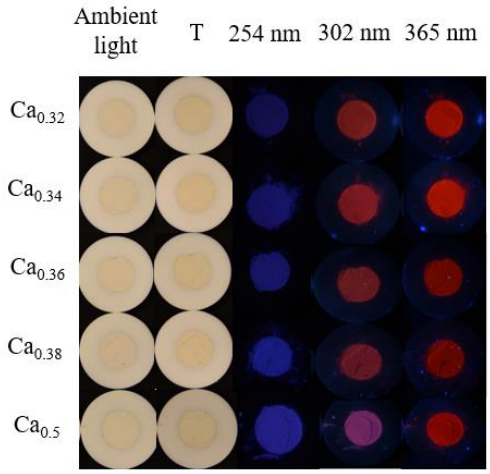

Figure 7. Photographs taken under different conditions of samples made using different amounts of sodium and calcium chlorides (T = tenebrescence).

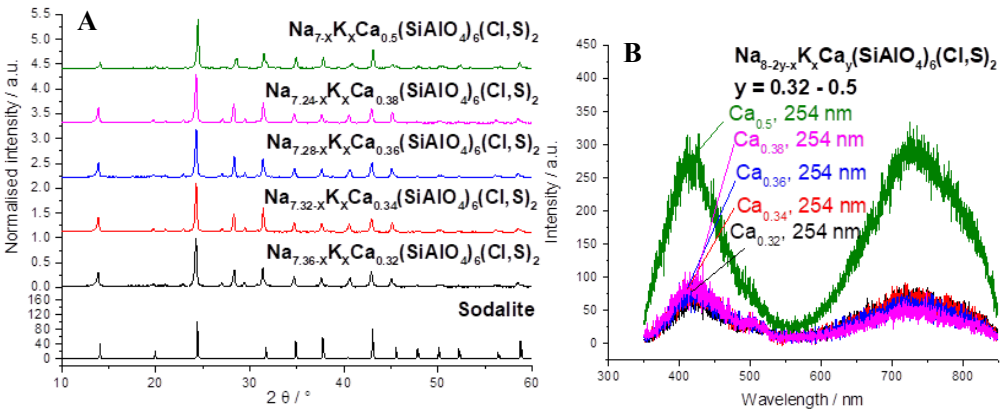

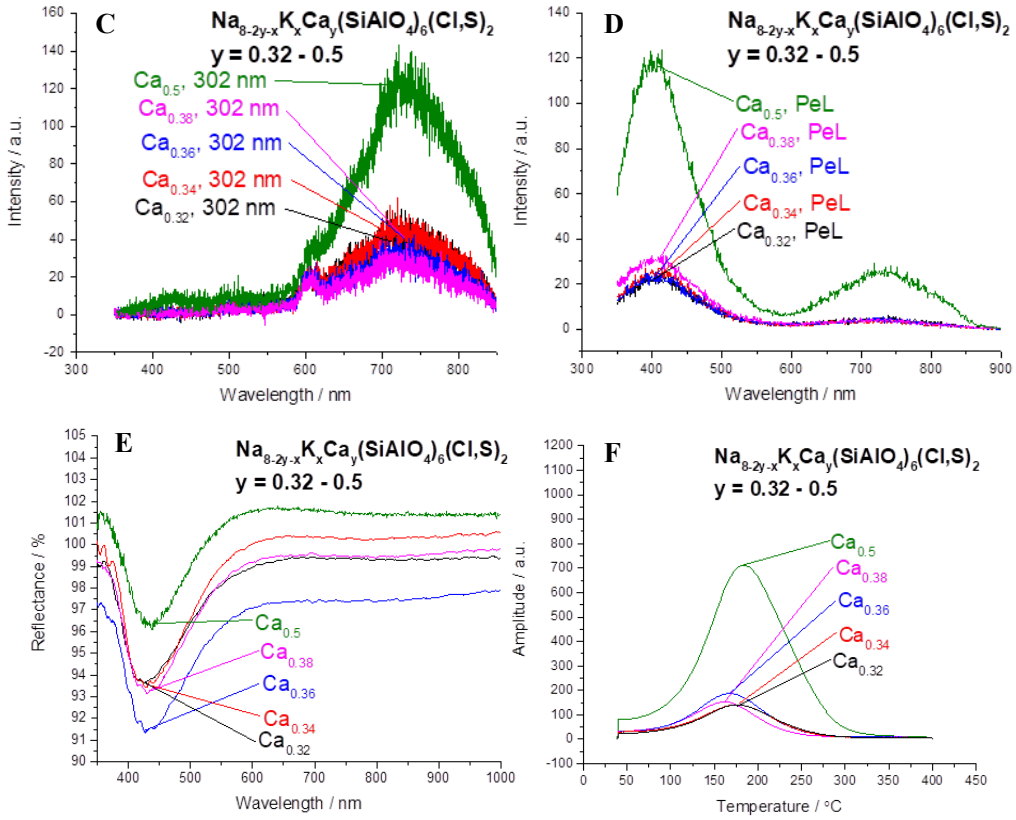

Figure 8. XRD graphs (**A**), emission spectra under 254 nm UV irradiation (**B**) and under 302 nm UV irradiation (**C**), PeL spectra (**D**), reflectance spectra (**E**) and TL glow curves (**F**) of samples made using different amounts of sodium and calcium chlorides. PeL, reflectance and TL were measured with an irradiation time and wavelength of 5 min and 254 nm, respectively.

3.4 Ca-exchanged samples showing NIR tenebrescence

It was noticed earlier that some samples had NIR tenebrescence i.e., an absorption in the NIR region after exposure to UV irradiation. This was a novel discovery, so it was investigated further by using various amounts of calcium chloride as starting material.

All the samples showing NIR tenebrescence have a sodalite structure with similar impurities at 18.2°, 26.8°, 28.4°, 33.2° and 40.8°. Additionally, $Ca_{0.64}$ and $Ca_{0.7}$ samples have impurity peaks at 32.1°, 36.3° and 42.3° (**Figure 9A**). When irradiated with 254 nm UV, samples have luminescence emission peaks at 420 nm and 725 nm with $Ca_{0.54}$ having less intense emission peaks than other samples. Additionally, $Ca_{0.64}$ and $Ca_{0.7}$ have emission peaks at 575 nm. Irradiating with 302 nm UV makes peaks at 420 nm less intense (**Figure 9B**). All the samples have relatively similar PeL spectra, having strong peaks at 405 nm and weaker peaks at 725 nm (**Figure 9C**). Interestingly, samples

have both yellow and NIR tenebrescence, having F-centre absorption bands centring at 425 nm and 905 nm (**Figure 9D**).

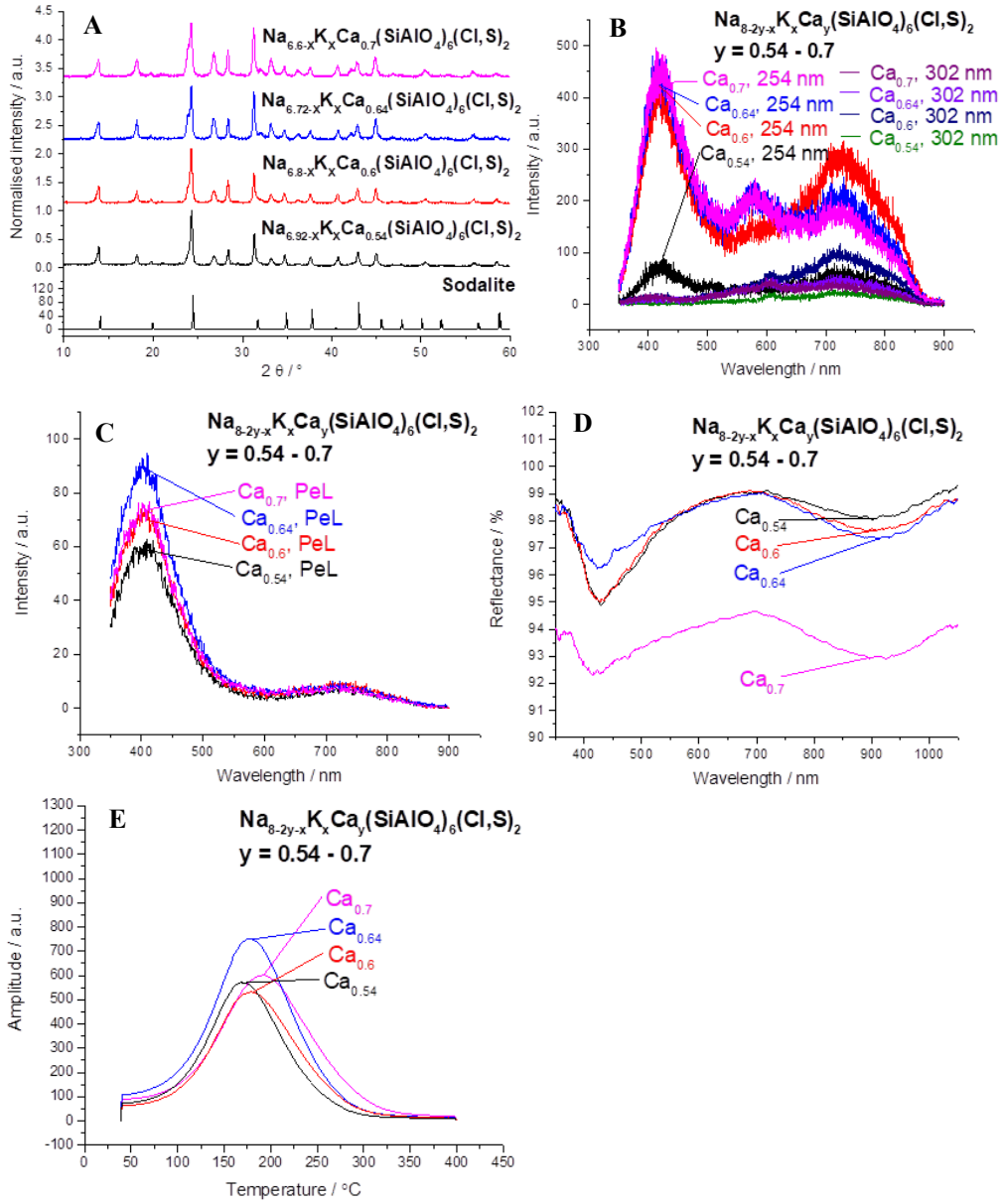

Figure 9. XRD graphs (**A**), emission spectra (**B**), PeL spectra (**C**), reflectance spectra (**D**) and TL glow curves (**E**) of samples made using different amounts of sodium and calcium chlorides. PeL, reflectance and TL were measured with an irradiation time and wavelength of 5 min and 254 nm, respectively.

3.5 Ion-exchanged samples

Finally, various ion-exchange syntheses were performed as explained in the Experimental section. Only products made from solid-state ion-exchanged materials resulted in hackmanite materials. Therefore, only these are presented below.

Each sample has a sodalite structure according to the XRD graphs. The K-ion-exchanged sample has impurity peaks at 21.1°, 23.0° and 27.0°. The Ca-ion-exchanged samples have impurity peaks at 21.1°, 23.0°, 27.0°, 29.5° and 38.8° and have a more intense peak at 45.0°. Additionally, $Ca_{0.58}$ sample has impurity peaks at 25.2° and 29.0°, the $Ca_{0.34}$ sample has impurity peaks at 29.0° and 38.2° and the $Ca_{0.12}$ sample has impurity peaks at 20.4°, 30.9° and 38.2° (**Figure 10A**). The K-ion-exchanged sample has luminescence emission peaks at 465 nm when excited with either 254 nm or 302 nm UV irradiation. The $Ca_{0.12}$ sample has two emission peaks at 465 nm and 500 nm when excited with 254 nm UV irradiation, the former being also the only peak when excited with 302 nm UV irradiation. The $Ca_{0.34}$ sample has a luminescence emission peak at 455 nm with both irradiation wavelengths, in addition to a peak at 580 nm when excited with 254 nm UV irradiation. The $Ca_{0.58}$ sample has only weak emission peaks (**Figure 10B**). The K-ion-exchanged sample shows PeL at 485 nm, while $Ca_{0.12}$, $Ca_{0.34}$ and $Ca_{0.58}$ samples have PeL peaks at 470 nm, 430 nm and 405 nm, respectively (**Figure 10C**). All samples show tenebrescence, K-ion-exchanged sample having an F-centre absorption band centring at 530 nm and $Ca_{0.12}$, $Ca_{0.34}$ and $Ca_{0.58}$ samples having F-centre absorption bands centring at 506 nm, 520 nm and 530 nm, respectively (**Figure 10D**). Tenebrescence and emission colours can also be seen in **Figure 10F**.

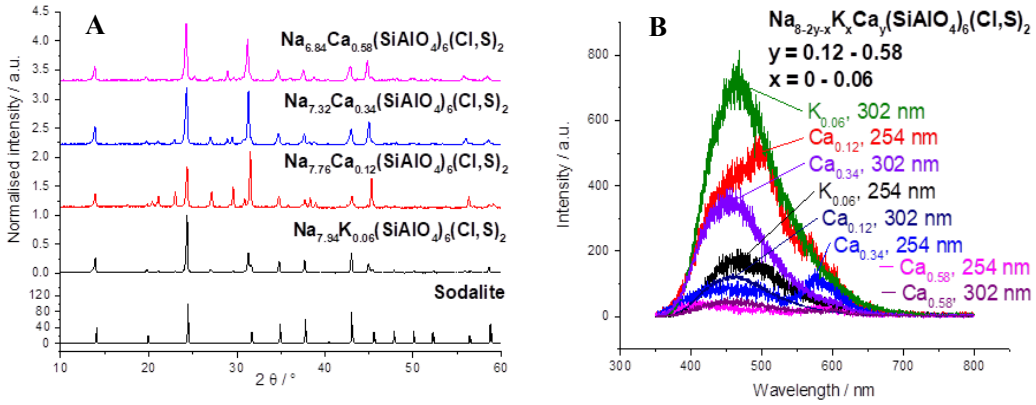

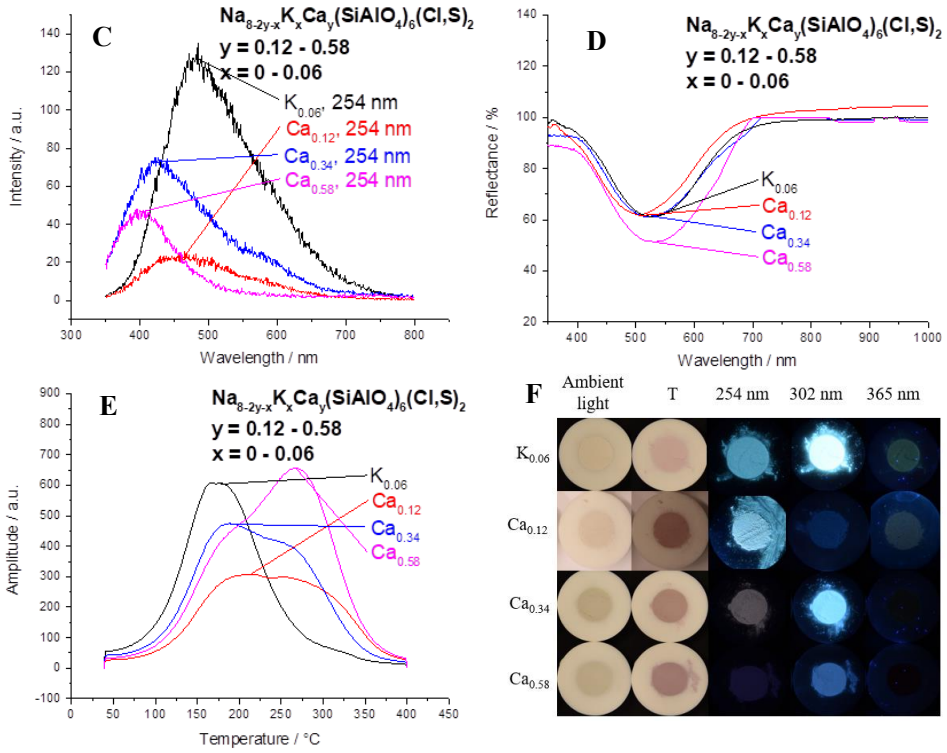

Figure 10. XRD graphs (**A**), emission spectra (**B**), PeL spectra (**C**), reflectance spectra (**D**), TL glow curves (**E**) and photographs taken under different conditions (T = tenebrescence) (**F**) of samples made using a solid-state ion-exchange reaction. PeL, reflectance and TL were measured with an irradiation time and wavelength of 5 min and 254 nm, respectively.

3.6 Rietveld refinement results and CIE *L*a*b* colour coordinates

Table 1 shows the *a* unit-cell parameters obtained from Rietveld refinements. Additionally, the difference between *a* unit-cell parameter of a hackmanite and the samples is presented, which shows that some samples have increased and decreased unit-cell sizes. Due to having impurity peaks in the XRD graphs, Rietveld refinements of some samples could not be performed, and, thus, are presented in the table as "n/a". Furthermore, CIE *L*a*b* colour coordinates of samples showing tenebrescence are presented in **Table 1**.

Table 1. Sample *a* unit-cell parameters obtained from Rietveld refinements compared to the *a* unit-cell parameter of a hackmanite[10] and CIE *L*a*b* colour coordinates of samples showing tenebrescence.

Nominal formula	*a* unit-cell parameter / Å	Parameter difference / Å	*L*	*a*	*b*
$Na_{8-x}K_x(SiAlO_4)_6(Cl,S)_2$	8.8848	-0.0022	61.91	29.03	-22.31
$Na_{7-x}K_{1+x}(SiAlO_4)_6(Cl,S)_2$	n/a	n/a	89.63	-0.47	3.38
$Na_{7-x}K_xLi_1(SiAlO_4)_6(Cl,S)_2$	8.7946	-0.0924	n/a	n/a	n/a
$Na_{7.75-x}K_{0.25+x}(SiAlO_4)_6(Cl,S)_2$	8.8861	-0.0009	58.19	13.82	-6.46
$Na_{7-x}K_xCa_{0.5}(SiAlO_4)_6(Cl,S)_2$	8.8881	0.0011	88.95	0.41	9.89
$Na_{7.75-x}K_xLi_{0.25}(SiAlO_4)_6(Cl,S)_2$	8.8801	-0.0069	63.43	14.39	-7.14
$Na_{7-x}K_xMg_{0.5}(SiAlO_4)_6(Cl,S)_2$	8.8960	0.0090	52.59	10.41	-8.23
$Na_{7-x}K_xSr_{0.5}(SiAlO_4)_6(Cl,S)_2$	8.9082	0.0212	n/a	n/a	n/a
$Na_{7-x}K_xBa_{0.5}(SiAlO_4)_6(Cl,S)_2$	n/a	n/a	67.43	1.13	1.35
$Na_{7.75-x}K_xRb_{0.25}(SiAlO_4)_6(Cl,S)_2$	n/a	n/a	47.39	14.53	-12.78
$Na_{4-x}K_xCa_2(SiAlO_4)_6(Cl,S,I)_2$	n/a	n/a	72.32	6.88	-2.34
$Na_{4-x}K_xCa_2(SiAlO_4)_6(Cl,S,Br)_2$	8.9812	0.0942	84.73	-2.11	-8
$Na_{4-x}K_xCa_2(SiAlO_4)_6(Cl,S,PO_4)_2$	n/a	n/a	88.61	0.12	1.9
$Na_{7.32-x}K_xCa_{0.34}(SiAlO_4)_6(Cl,S)_2$	8.8828	-0.0042	87.83	1.31	12.49
$Na_{7.28-x}K_xCa_{0.36}(SiAlO_4)_6(Cl,S)_2$	8.8446	-0.0424	88.12	1.02	11.11
$Na_{7.24-x}K_xCa_{0.38}(SiAlO_4)_6(Cl,S)_2$	8.8820	-0.0050	88.14	1.27	11.26
$Na_{6.92-x}K_xCa_{0.54}(SiAlO_4)_6(Cl,S)_2$	8.8938	0.0068	n/a	n/a	n/a
$Na_{7.76}Ca_{0.12}(SiAlO_4)_6(Cl,S)_2$	n/a	n/a	67.7000	15.82	-3.71
$Na_{7.32}Ca_{0.34}(SiAlO_4)_6(Cl,S)_2$	n/a	n/a	57.6500	15.38	-4.83
$Na_{6.84}Ca_{0.58}(SiAlO_4)_6(Cl,S)_2$	8.9074	0.0204	51.2400	18.87	-10.35
$Na_{7.94}K_{0.06}(SiAlO_4)_6(Cl,S)_2$	8.8744	-0.0126	67.88	17.65	-10.61

4 Discussion

4.1 Sample purity

Most samples have a sodalite structure according to the XRD graphs presented in the Results section. Samples, which showed no sodalite structure, for instance samples doped with F^-, CO_3^{2-} or PO_4^{3-}, were not further analysed. Additionally, XRF results (Supporting Information) show that samples, which have a sodalite structure, have an elemental structure with various amounts of Na, Al, Si, S and Cl, which are typical elements for sodalite. Additionally, most samples have various amounts of K due to the starting reagent containing potassium and small traces of different impurities including Fe. Furthermore, most samples with a sodalite structure show either characteristic luminescence or tenebrescence properties for hackmanites, which are further analysed in the chapters 4.2 and 4.3.

Impurity peaks of the samples with a sodalite structure were further analysed. Peaks at 20.9°–21.0°, 22.8°–22.9° and 29.4° were common impurity peaks for most samples and can be identified as nepheline[58a], $Na_3KAl_4Si_4O_{16}$. Nepheline is an aluminosilicate with weak optical properties[33] and has been previously reported to formulate during solid-state sodalite synthesis by Byron et al.[20]. Although they concluded that the forming of nepheline was due to increased heating temperature in the synthesis, this is not the case this time since the heating temperature was kept constant during the synthesis. However, most likely explanation for nepheline traces is the potassium coming from the starting reagent, since the sample made from other starting reagents did not show nepheline impurity peaks. Increased amount of potassium at the beginning of the synthesis could lead to partial formation of nepheline instead of fully forming to sodalite. Additionally, nepheline can form if there is a deficiency of halogen in the structure, for instance, if not enough halogen salts were used as starting material or if the halogen was too large or unwilling to react to get the right amount into the structure[33]. The size of the halogen could explain why using F^-, CO_3^{2-} or PO_4^{3-} salts as starting materials resulted in a lot of impurities instead of clean sodalite structure.

Another two common impurity peaks for these samples were peaks at 27.0° and 45.2°, and peaks at 28.1°–28.4° and 40.7°–40.8°, which could be identified originating from NaCl[58b] and KCl[58c], respectively. Peaks at 40.7°–40.8° were also identified as KCl. Additionally, Ba-exchanged sample had impurity peaks at 22.2° and 39.7, which were identified as $BaCl_2$[58d], while the impurity peak of Br-doped sample at 29.0° was identified as $CaBr_2$[58e]. These impurity peaks originate from excess amounts of salts used in this synthesis to achieve sodalite structures. Additionally, KCl could be formed due to excess amount of chloride ions coming from salts and potassium coming from the main starting reagent. Salt impurities can be washed away with water, although this weakens the yellow and NIR tenebrescence slightly, as described in **Figure 11**. The washed products were dried at 500 °C, which can result in decrease of tenebrescence colour intensity due to sulphur species starting to oxidize again that could explain the weakening of the yellow and NIR tenebrescence of the washed products.

XRF results (Supporting Information) also showed that cation exchanged samples had their respective cations in the elemental structures. However, this does not entirely prove that the exchanged cations have entered the sodalite structures since XRF

results could also show salt impurities outside the structures and the cation exchanged samples were mostly not washed.

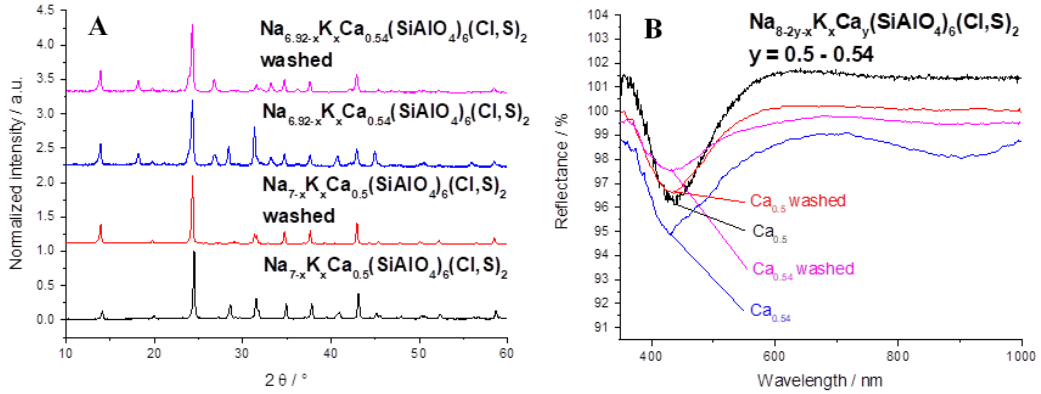

Figure 11. XRD graphs (A) and reflectance spectra (B) of unwashed and washed Ca-exchanged hackmanites.

4.2 Luminescence properties

Natural hackmanites usually show emission peaks at orange, green/blue or red area depending on the excitation wavelength and the origin of the sample[3] while the luminescence properties of synthetic hackmanites are highly dependent on the elemental composition of the material[3,6,7]. The luminescence properties of natural and synthetic hackmanites have been presented thoroughly in the Introduction section.

When Na^+ ions were partly replaced with either Ca^{2+}, Mg^{2+}, Ba^{2+} or Sr^{2+} ions, shifts in the emission peaks were noticed (**Figure 4BC**). Common for samples containing calcium was that they show sharper emission peak at 415 nm and a broader

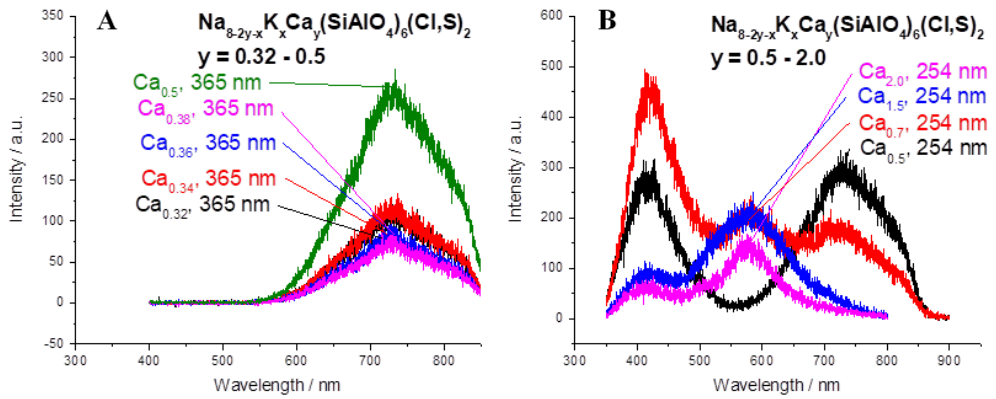

Figure 12. Emission under 365 nm UV irradiation (**A**) and emission under 254 nm UV irradiation (**B**) of samples containing different amounts of calcium.

emission peak at NIR area peaking at 735 nm with excitation at 254 nm (**Figure 8B**). Excitation with higher wavelengths 302 nm and 365 nm resulted in emission peaks only in the NIR area (**Figure 8C** and **Figure 12A**). With increasing amounts of calcium, the emission peaks at 415 nm and NIR area become weaker or even unnoticeable and an emission peak at 580 nm arises (**Figure 12B**). Henderson et al.[34] reported that F^+ centres in calcium oxide create emission at 382.2 nm while F centres in calcium oxide create emission at 627 nm. Having emission peaks at 415 nm and knowing that blue emission originates from O_2^- entities[19], could possibly mean that some of the Ca^{2+} ions have replaced either Al^{3+} or Na^+ ions in the sodalite structure leading to creation of oxygen vacancies and F^+ centres. Broad emission peak at NIR area could originate from two emission peaks: the first emission peak beginning at 600 nm originating from either S_2^- luminescence centre[17] or F centres created by substitution of Ca^{2+} ions into the sodalite structure. The second emission peak at 735 nm is likely to originate from Fe^{3+} substituting for Al^{3+} in tetrahedral sites[18], since all the calcium-exchanged sodalite samples contain iron impurities and only few samples contain chromium impurities (**Table S 5**, Supporting Information).

Yellow photoluminescence, with an emission peak at 560 nm, was detected, when Na^+ ions were partly replaced with Ba^{2+} ions (**Figure 4BC**). It has been previously reported that carbon dots doped with Zn^{2+} ions can emit yellow photoluminescence[35] while Eu^{2+} is also a known yellow phosphor[36]. Furthermore, yellow photoluminescence has also been achieved by Cu^+ doping of phase-separated glasses in alkali borosilicate systems, where yellow photoluminescence was attributed to formation of Cu^+ clusters[37]. In fact, according to XRF results (**Table S 2**, Supporting Information), there are both zinc, copper and europium impurities in the $Ba_{0.5}$ sample showing yellow photoluminescence. Additionally, another sample containing europium and copper impurities and no zinc impurities (**Table S 3**, Supporting Information), CO_3 doped sample, also showed yellow photoluminescence at 580 nm. Therefore, the luminescence centre could be either Eu^{2+} or Cu^+ ions, which could be further investigated in the future. Needless to say, having Eu^{2+} ions as luminescence centres is not ideal for hackmanites, having no lanthanides being a positive for them. Furthermore, introducing different ions, like $Ca^{2+}$and CO_3^-, could create small changes in the hackmanite structure and the energy levels of hackmanites and, thus, change the transitions that occur during luminescence emission. Therefore, the luminescence centres would remain the same as in normal hackmanite, while showing different emission colours.

Mg, Li, and Sr-exchanged samples all show bright blue emission peaks at 450–460 nm (**Figure 3B** and **Figure 4BC**), which likely originate from O_2^- entities[19]. Additionally, the Sr-sample shows an emission peak at 385 nm, which could mean that Sr^{2+} ions could replace Al^{3+} ions in the sodalite structure leaving an oxygen vacancy leading to creation of F^+ centres known for creating emission at shorter wavelengths. Furthermore, Gao et al.[38] have showed that doping with bromine can enhance luminescence properties of certain phosphors. While Mg, Li, and Sr-exchanged samples all have bromine impurities, as per XRF data (**Table S 2**, Supporting Information), the Br-doped and Ca-exchanged hackmanite sample showed intense blue emission at 410 nm (**Figure 6B**), which could possibly mean that bromine acts as blue photoluminescence enhancer in hackmanites too. Norrbo et al.[7] also explained that the bright emission of hackmanites can be obtained by replacing Na partly with Li, since the materials show only negligible photochromism with Li present due to increase in the splitting of ground and excited levels of the disulphide ion because of stronger crystal field caused by the compression of the structure. When Na of the sodalite samples is partly replaced with a large enough amount of Li, Sr, Ba or Ca ions the samples lose the traditional purple tenebrescence of hackmanites and, thus, show more intense photoluminescence and PeL.

Hackmanites usually show PeL emission peaks at 460 nm[3,6,20] or at 500 nm[9] upon Ti doping. While Li, Mg and Sr-exchanged samples showed PeL emission peaks at around 460 nm (**Figure 3C** and **Figure 4D**), Ca and Ba-exchanged samples show PeL emission peaks at 400 nm and 385 nm, respectively (**Figure 4C**, **Figure 6C**, **Figure 8D** and **Figure 9C**). PeL in hackmanites has been previously assigned to originate from the Ti^{3+}–V_0 pair[9], however, only some Ca-exchanged samples and the Ba-exchanged sample showed titanium impurities in the XRF data (**Table S 2**, **Table S 3** and **Table S 4**, Supporting Information). However, Agamah et al.[3] explained that XRF can only measure in a micrometre scale resolution and, thus, there might some elements missing. They also reported that there is interplay between potassium and sulphur, which affects the tenebrescence and PeL properties of hackmanite. When no potassium atoms are present, there is a high overlap between the S_2^- band causing tenebrescence and the absorption band of Ti^{3+} that associates with PeL, thus, weakening the PeL intensity. The overlap decreases when potassium atoms are present in the structure and, therefore, the competition between PeL and tenebrescence becomes weaker leading to stronger PeL intensity. All hackmanite samples made from starting reagent containing potassium have high amounts of potassium and low amounts of sulphur (see XRF results in Supporting

Information), which can lead to an increase in PeL intensity. There is also a clear pattern between samples showing purple tenebrescence and having weak PeL intensity (**Figure 4DE**), which fits the theory of interplay between sulphur and potassium explained by Agamah et al.[3].

Blue PeL has been previously reported for samples containing Eu^{2+} as luminescence centres[39,40] and this PeL was assigned to originate from the relaxation from Eu^{2+} 5d excited state to the 4f ground state. However, PeL from Eu^{2+} peaks at 430–460 nm, while Ca and Ba-exchanged hackmanites synthesized in this work had PeL peaks at 400 nm and 385 nm, respectively. Ming et al.[41] also reported blue PeL at 385 nm and assigned this to the transition of $^5D_3 \rightarrow {}^7F_6$ of Tb^{3+}. Although some Ca and Ba-exchanged hackmanites show europium and terbium impurities (**Table S 3** and **Table S 4**, Supporting Information), there is no clear pattern between these impurities and showing blue PeL, since some Ca-exchanged hackmanites show blue PeL even without having these impurities. Therefore, it is more probable that blue PeL in these hackmanites also originates from electrons being trapped in oxygen vacancies in the vicinity of Al^{3+} suggested being the place where UV/blue photoluminescence is created[3]. The blue-shift in Ba-exchanged sample could be explained by ionic radius of Ba^{2+}; being larger than Ca^{2+} ion means that there will be an increase in bond lengths near the luminescent centre, which results in decrease in bond lengths of the luminescent centre. This, in turn, leads to greater energy difference between the excited and ground state of the luminescent centre, which shifts the PeL emission peak to lower wavelengths.[40]

Interestingly, some samples, most notably $Ca_{0.5}$ and $Ba_{0.5}$-exchanged samples, show red PeL (**Figure 4D**) with broad peaks at NIR area peaking at around 730 nm. Cr^{3+} ions[42] and Fe^{3+} ions[43] are well-known to be able to emit PeL at NIR regions. As explained before, Fe^{3+} is more likely to be the source of red photoluminescence and PeL, since nearly all of the samples contained iron impurities (see XRF results in Supporting Information). Zeng et al.[43] suggested that NIR emission originates from the spin-forbidden $^4T_1 \rightarrow {}^6A_1$ transition of Fe^{3+} and the excitation band for PeL originates from $O^{2-} \rightarrow Fe^{3+}$ charge transfer after the substitution of Fe^{3+} to Al^{3+}.

Another possible luminescence centre[17] could be S_2^- and it has been reported that, under lower temperatures, instead of having one broad emission peak from around 600–800 nm, multiple narrow emission peaks emerge originating from the S_2^- luminescence centre.[17,18] Therefore, some samples showing red PeL were cooled down using liquid nitrogen and PeL spectra were measured using Avantes SensLine AvaSpec-HS-TEC spectrometer connected with an optical fibre (**Figure 13**). Red PeL could not be observed in 77 K, which could be due to different measurement setup or structural changes in lower temperatures. Further investigations are needed to determine whether this red PeL originates from either S_2^- or Fe^{3+} luminescence centres or whether it originates from something else.

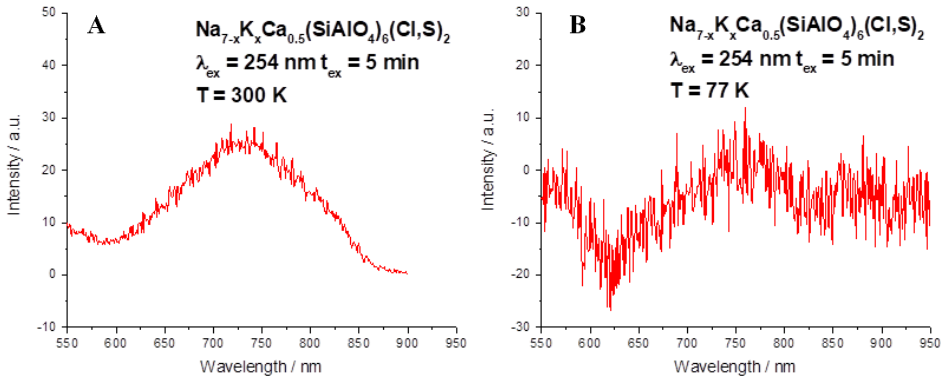

Figure 13. PeL spectra in higher wavelengths in 300 K (A) and 77 K (B).

4.3 Tenebrescence properties

Tenebrescence occurs when electrons are trapped in defect energy levels in the bandgap and F-centres are formed. Tenebrescence in hackmanites is known to arise from chlorine vacancies that capture electrons originating from electron-rich sulphur-ions after irradiation with UV or X-ray radiation.[9] Detailed information and the mechanism of tenebrescence has been presented in the Introduction -chapter. Previously, natural hackmanite[3] has been reported to show purple tenebrescence with F-centre absorption band centring at 550 nm while synthetic hackmanites, produced with either solid-state reaction from zeolite A[6] and zeolite-free synthesis[20] or microwave-assisted synthesis[28], have also shown purple tenebrescence with F-centre absorption bands centring at 550 nm

or 530 nm, respectively. Purple tenebrescence was achieved for samples made from only sodium salts and K, Mg, Li and Rb-exchanged samples (**Figure 4E**). Interestingly, some Ca-exchanged materials show yellow tenebrescence with an F-centre absorption band centring at 425 nm (**Figure 8E**) and NIR tenebrescence with an F-centre absorption band centring at 905 nm (**Figure 9D**), while Ca-exchanged material doped with bromine shows light blue tenebrescence with an F-centre absorption band centring at 615 nm (**Figure 6D**). Light blue tenebrescence has been previously found in scapolite, an aluminosilicate forming solid solutions between marialite ($Na_4Al_3Si_9O_{24}Cl$) and meionite ($Ca_4Al_6Si_6O_{24}CO_3$), with the light blue colour originating from a 628 nm absorption band, which is close to an absorption band of S_3^- trimer at 594 nm.[44] There are no previous publications about yellow or NIR tenebrescence in hackmanites and, therefore, these properties are considered to be new for hackmanites.

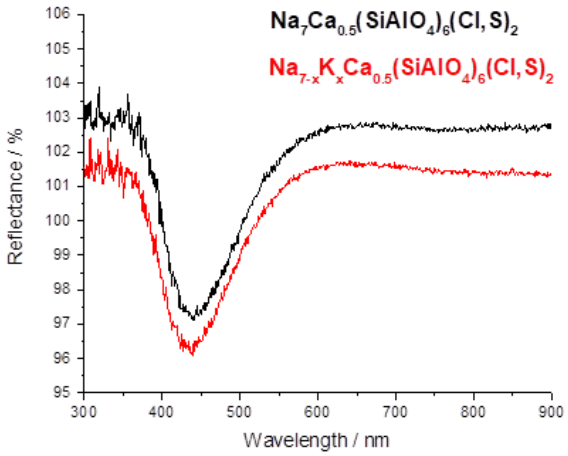

Figure 14. Reflectance spectra of samples made from various starting reagents showing yellow tenebrescence.

Compared to the hackmanites showing purple tenebrescence, hackmanites showing yellow tenebrescence are synthesized with calcium and potassium. However, a Ca-exchanged sample made from a starting reagent, which contains no potassium, also

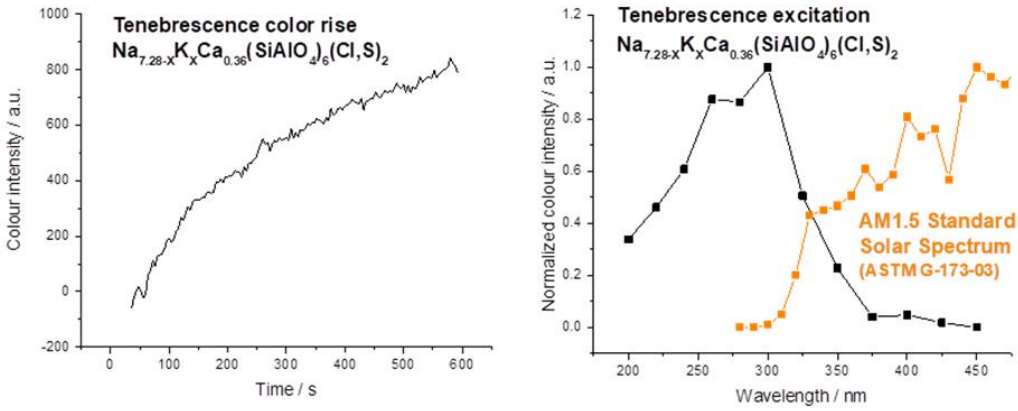

Figure 15. Tenebrescence colour rise curve and tenebrescence excitation spectrum of a hackmanite with yellow tenebrescence compared to the standard solar spectrum.

showed yellow tenebrescence (**Figure 14**). Therefore, it is believed that potassium is not a deciding factor, when yellow tenebrescence is concerned. The intensity of yellow colour increases with increasing time under UV irradiation, which indicates that the hackmanite showing yellow tenebrescence is suitable for quantification of UV doses (**Figure 15**). The yellow tenebrescence colour can also be bleached under natural light (**Figure 16**). Additionally, the tenebrescence excitation curve shows that the yellow tenebrescence colour can be obtained with irradiation wavelengths at 200–360 nm and, according to AM1.5 Standard Solar Spectrum, there is around 60 nm overlap with the sun's spectrum (**Figure 15**). This means that the colour of the materials showing yellow tenebrescence could also change colour in sunlight. Compared to the tenebrescence excitation spectra[8] of a traditional hackmanite and K and Rb-exchanged hackmanites, which have tenebrescence excitation peaks at 225 nm, 275 nm and 250 nm, respectively, Ca-exchanged hackmanite shows tenebrescence excitation peak at a longer wavelength at 300 nm. Additionally, the colouration of the material occurs in excitation range of at least 200–360 nm, which is broader compared to the excitation range of 225–290 nm of a traditional hackmanite[9].

One suggestion of causing yellow tenebrescence is that calcium could partly replace sodium in the sodalite structure, resulting structural changes and making the formed F-centres absorb higher energy photons at 2.9 eV instead of photons at the 2.3 eV which gives hackmanites the purple colour. Norrbo et al.[8] explained that K or Rb dopants in the sodalite structure are in close proximity of the chlorine vacancy, which leads to reduction of the energy gap between $a_1(V_{Cl})$ and $\pi^*(S_2^{2-})$ and a lower activation energy, which causes the F-centre to shift to higher wavelengths. Ca dopants could have a similar effect, although instead of decreasing the activation energy, the activation energy would increase. An increase in activation energy was noticed when Li dopants were introduced to the sodalite structure[8]. However, the F-centre shift caused by K or Rb dopants was only around 15 nm, while Ca dopants

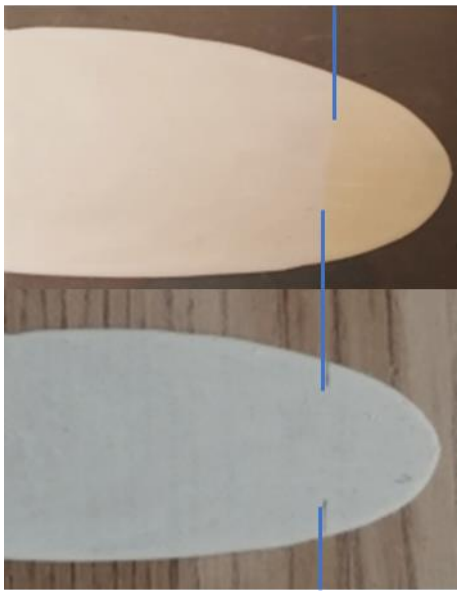

Figure 16. Yellow tenebrescence colour after 5 min UV irradiation under 254 nm (top) and the same material after 72 h bleaching under daylight (bottom). The material has been tape-cast and the blue lines are showing the edge between irradiated and non-irradiated area.

cause a shift more than 100 nm, which could mean that something else causes yellow tenebrescence.

It is worth noting that while introducing calcium into the sodalite structure, it was expected that the synthesized materials would have similar properties to traditional hackmanite, since Ca^{2+} and Na^{+} ions are similar in size. For low Ca concentrations that is the case (**Figure S 1**, Supporting Information), however, once the Ca concentration reaches a certain point, which, in this case, was 16 % of the used salts (corresponding to a structure of $Na_{7.4-x}K_xCa_{0.3}(SiAlO_4)_6(Cl,S)_2$), the tenebrescence colour switches from purple to yellow. However, once the Ca concentration goes above 50 % of the used salts, the tenebrescence colour disappears completely (**Figure S 2**, Supporting Information). This observation could mean that once the amount of calcium in the structure is $Ca_{0.32–1.0}$ the calcium changes the structure enough to shift the tenebrescence peak to yellow, or maybe that amount is required for a possible second mechanism to dominate.

As explained earlier, white/gray-yellow tenebrescence in hackmanites has not been reported earlier, although Yang et al.[45] managed to produce a transparent ferroelectric ceramic, 0.85 $K_{0.5}Na_{0.5}NbO_3$ - 0.1 $ZrSrO_3$:0.005 Sm^{3+}, behaving the opposite way; showing yellow-gray reversible photochromism upon 420 nm irradiation. They concluded that the photochromism mechanism was due to decrease of reflectivity of the ceramic after excitation of high-energy photons and electron movement between valence band and defects of V'_O and hole capturing by the defects of V'_{Na} and V'_K. The reversible process is then achieved by thermal stimulus. Although reversible photochromism shown by this material is closely related to the tenebrescence shown by hackmanites presented in this thesis, the composition of the ceramic material differs a lot from the composition of hackmanite and reversible photochromism in the ceramic material was achieved by using much lower energy photons (2.95 eV) compared to ones used to achieve tenebrescence in hackmanites (3.40–4.88 eV). Thus, no further conclusions can be drawn from the reversible photochromism shown by the ceramic material.

NIR photochromism has been found earlier in organic molecules in various solvents and these materials have potential in applications as photoswitches or biosensors.[46,47] Additionally, molybdenum based inorganic pigments, $RE_6Mo_2O_{15}$ (RE = Tb, Dy, Er, Ho), have shown a change in NIR reflectivity under various lamps.[48] However, this change in NIR reflectivity cannot be classified as tenebrescence, since the NIR reflectivity change is due to changes in the spectra of different lamps, which leads

to sample reflecting differently under various lamps. Additionally, NIR photochromism in these papers was achieved upon irradiation with longer wavelength light sources, mostly operating in the visible light wavelengths (400–700 nm), while Ca-exchanged hackmanite materials showed NIR photochromism under 254 nm UV light irradiation (**Figure 17**). Worth noticing is that all the described materials showing NIR photochromism are yellow, whether liquid or solid. This also applies to the Ca-exchanged hackmanite showing NIR tenebrescence, since it simultaneously shows yellow tenebrescence (**Figure 9D**). Whether yellow colour of the material is important in achieving NIR tenebrescence cannot fully be confirmed based on currently available information. However, reflectance spectra presented in **Figure 9D** show that $Ca_{0.6}$ and $Ca_{0.54}$-exchanged materials have relatively similar intensities of the F-centres at 425 nm, suggesting that they are equally yellow, while the former material has deeper NIR absorbance at 905 nm. This suggest that yellow colour has only little effect on NIR tenebrescence, while the increased amount of calcium in the material results in deeper NIR tenebrescence. However, once the amount of calcium increases by larger margin, NIR tenebrescence does not appear anymore (**Figure S 2**, Supporting Information) suggesting that there is a certain limit in the amount of calcium, which makes NIR tenebrescence deeper. Thus, further investigations are needed to fully understand the mechanism behind NIR tenebrescence in hackmanites.

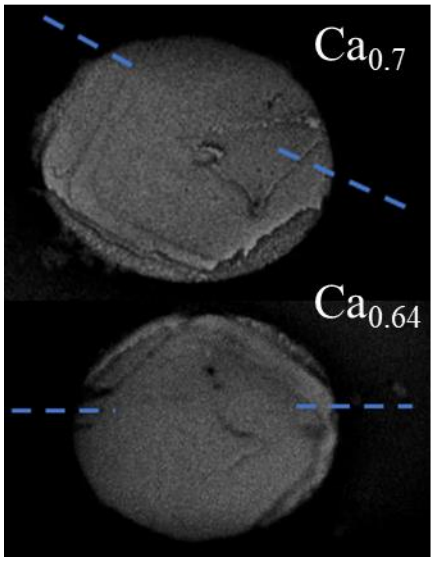

Figure 17. Photographs showing NIR tenebrescence under solar light simulator and >820 nm IKS5 filter after 15-minute 254 nm UV irradiation. The irradiated area can be seen as darker area above the blue dotted line. (Original photograph taken by Hannah Byron)

4.4 Potential applications

Based on the luminescence properties of hackmanites, they have been proposed as potential materials for, for example, optical markers, sensors, multiplexing in diagnostics and exit signs.[6,7,9] Additionally, the photochromism properties could be utilized in bioimaging, optical data storage and colour changing eyeglasses[6,8,9]. Only recently, Vuori et al.[49] also proposed a new technique in the detection of X-ray doses with colour-changing hackmanites, which could be used in industrial imaging or dosimetry. However, based on the unique properties found in Ca-exchanged hackmanites, mainly NIR emission and tenebrescence and yellow tenebrescence, three potential applications are presented in

the following chapters: applications in anti-counterfeiting, UV dose determination and luminescence down shifting in photovoltaic systems.

4.4.1 Anti-counterfeiting

Anti-counterfeiting materials can be both inorganic[23] and organic[22] and can have multiple properties based on luminescence and photochromism, making them possible to be used in multimode anti-counterfeiting applications.[24–26] These materials have been presented thoroughly in the Introduction section.

Considering all the materials described in the Introduction section, Ca-exchanged hackmanites, particularly $Ca_{0.5}$-exchanged hackmanite, shows excellent properties for advanced, multidimensional anti-counterfeiting applications. Firstly, the material shows various emission colours under different wavelength UV light: blue under 254 nm, purple under 302 nm and red under 365 nm. The purple colour is the result of both the red and blue colour being excited simultaneously. Secondly, the material shows blue PeL after 254/302 nm UV irradiation. Thirdly, the material shows yellow photochromism after 254 nm UV irradiation. Yellow photochromism is also likely to be achieved after 302 nm UV irradiation, since the tenebrescence excitation spectra (**Figure 15**) shows that the most intense colour is achieved after excitation close to 300 nm, although this was not tested in this work. These luminescence and photochromism properties of the $Ca_{0.5}$-exchanged hackmanite already show a total of six different properties that are easily achievable using hand-held UV lamps and can be verified with naked eye making them useful in advanced anti-counterfeiting applications. Furthermore, mechanochromism, UC-PL or temperature-dependent luminescence were not tested in this work. If these properties would be introduced through the use of dopants[16] in the $Ca_{0.5}$-exchanged hackmanite, it would make the total amount of properties suited for advanced anti-counterfeiting applications even higher. Properties shown by $Ca_{0.5}$-exchanged hackmanite suitable for advanced anti-counterfeiting applications are shown in **Figure 18** Finally, NIR tenebrescence of some Ca-exchanged hackmanites could be used in anti-counterfeiting to achieve an invisible anti-counterfeiting application, since NIR tenebrescence cannot be seen by naked eye. Using cameras and different filters, like those used in taking photographs showed in **Figure 17**, could also make it easily achievable, although using spectrometers would be advisable to obtain reliable results, which could make the anti-counterfeiting applications based on NIR tenebrescence less accessible in certain places.

A couple of possible obstacles still need to be addressed before Ca-exchanged hackmanites can be truly considered as possible materials for anti-counterfeiting applications. Firstly, the luminescence and photochromism properties of the material must be tested in different solutions like water, polyvinyl alcohol and other organic solutions to be able to produce inks, which would be suitable for anti-counterfeiting applications on banknotes[24,25]. Tape-casting of hackmanites has already proven that the photochromism properties of the material remain after adding different amounts of organic solutions to the material, while Norrbo et al.[7] showed that Li-exchanged hackmanite is extremely stable in aqueous media and the emission bands could be detected in the nanomolar range. These results are positive, when Ca-exchanged materials are considered to be used as materials in anti-counterfeiting applications. Secondly, the storage and thermal stability tests could be carried out similarly as Xu et al.[26] did. Finally, proper performance tests of the luminescence and photochromism properties of these materials should be tested to see whether the photoluminescence and PeL intensities and photochromism colour intensity remains the same after multiple irradiation/bleaching cycles.

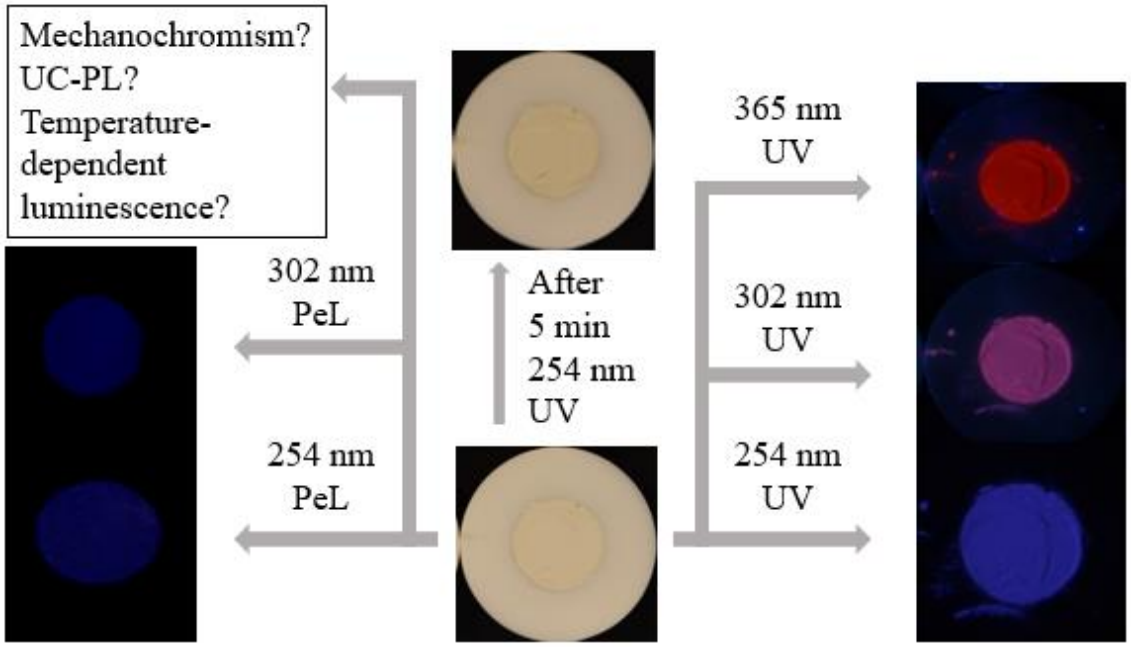

Figure 18. Luminescence and photochromism properties of $Ca_{0.5}$-exchanged hackmanite suitable for multimode advanced anti-counterfeiting applications. (PeL photographs taken by Hannah Byron)

4.4.2 UV dose and index determination

Norrbo et al.[8] investigated a possibilty of using hackmanites in UV index and dose determination. They showed that tenebrescence colour is dependent of the time of UV exposure, which also applies to Ca-exchanged hackmanites showing yellow

tenebrescence (**Figure 15**). Next, they showed that the thermal bleaching of the tenebrescence colour occurs at temperatures of 80 °C and above making optically stimulated bleaching only option for practical applications. They also stated that, since sunlight contains only a small amount of UV light and a larger amount of visible light that erases the colour of hackmanite caused by tenebrescence, it would be advisable to read the intensity of the colour as soon as possible after UV irradiation or during UV irradiation. However, they explained that a concentrating lens and a visible range blocking filter could be used in applications so that the UV dose detection response is more accurate. Finally, they showed that with these methods, UV dose and UV index can be determined from the intensity of the tenebrescence colour, making hackmanites suitable for applications in UV dosimetry.

Ca-exchanged hackmanites show yellow tenebrescence, which intensifies over longer UV exposure time and overlaps around 60 nm with the sun's spectrum (**Figure 15**) making it potentially suitable material for similar UV dosimetry applications presented by Norrbo et al.[8]. However, yellow colour change is harder to see by naked eye compared to the purple colour change of natural hackmanites. This could limit the amount applications that are suitable for Ca-exchanged hackmanites, although by introducing sensitive sensors to applications that can read and give the intensity of the colour, and, therefore, the UV dose and index, directly to the user, could solve this problem. In theory, by having larger spectral overlap to the sun's spectrum than traditional hackmanites, Ca-exchanged hackmanites could be even more sensitive to UV irradiation, which would make them more suitable to UV dosimetry applications. It would also be interesting to measure tenebrescence fading of Ca-exchanged hackmanites to see whether the tenebrescence colour fades in visible light as rapidly as the purple colour of traditional hackmanites.

4.4.3 Luminescent down shifting in photovoltaic systems

Solar energy is a renewable source of energy, where energy is transformed into electricity by photovoltaic conversion in solar cells. By some estimates, more than 90 % of today's solar cells are based on crystalline silicon (c-Si) with a band gap of 1.12 eV (1107 nm).[50] A band gap describes the minimum energy a certain type of solar cell needs to create an electron-hole pair, which eventually leads to energy conversion into electricity. Higher-energy photons generate hot carriers, which leads to thermalization and wasting energy of the photons as heat. Furthermore, lower-energy photons are not absorbed by the solar

cell and, therefore, cannot be converted into electricity. An increase in the temperature of the solar cell lowers the operating voltage and increases the current leading to a reduction of the solar cell electrical output.[51] Luminescent down shifting (LDS)[52] has been introduced to overcome the bad short-wavelength response of solar cells by absorbing UV and blue photons and emitting them at longer wavelengths near the band gap of the solar cell.[51]

Ca-exchanged hackmanites absorb photons between 365–570 nm under UV irradiation, with an absorption peak at 425 nm and emit photons between 590–860 nm with an emission peak at 735 nm (1.69 eV) under 302 nm UV irradiation (**Figure 8CE**). According to the AM1.5 Standard Solar Spectrum, the solar spectrum consists mainly of light wavelengths longer than 300 nm. Therefore, under sunlight, Ca-exchanged hackmanites mainly emit photons from red to NIR wavelengths, while being able to absorb photons at visible wavelengths. Thus, Ca-exchanged hackmanites could possibly be introduced in photovoltaic systems as LDS layers, where Ca-exchanged hackmanite phosphors are mixed in ethylene vinyl acetate (EVA), as presented by Alonso-Álvarez et al.[51] and in **Figure 19**. Since the photons emitted from Ca-exchanged hackmanites come still some 300–400 nm short of the bandgap of c-Si solar cells, these LDS layers could be more suitable for $CH_3NH_3PbI_3$ perovskite solar cells[53] or a-Si, CdTe and CIGS thin film solar cells[54] with higher energy band gaps of 1.55 eV (800 nm), 1.75 eV (708 nm), 1.44 eV (861 nm) and 1.0–1.6 eV (1240–775 nm), respectively.

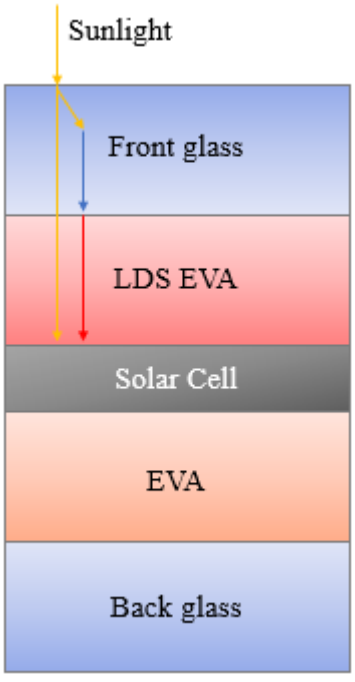

Figure 19. Possibly structure for solar cell system, where LDS layer is incorporated. The arrows present the photon flow in the photovoltaic system, with some of the visible radiation converted into NIR radiation.

Some challenges remain before LDS layers made from Ca-exchanged hackmanites could be incorporated to photovoltaic systems. Firstly, incorporating Ca-exchanged hackmanite into EVA or polymethyl methacrylate (PMMA), another common encapsulation material for LDS layers[51], should be tested to see whether the luminescence properties remain in this lattice. Even if an LDS layer composed of Ca-exchanged hackmanites could be built, the advantage of using such layers still remains a question. So far, limitations arising from poor absorption and, thus, spectral conversion efficiency have prevented the

predicted gain in solar cell efficiency.[55] Alonso-Álvarez et al.[51] also noticed only small differences in solar cell temperatures by using LDS layers in a photovoltaic system. Day et al.[55] also explained that using LDS layers makes photovoltaic systems more expensive and a proper financial comparison should be evaluated and new cost per watt peak calculated before making proposals for LDS layers. However, Ca-exchanged hackmanites are made of inexpensive, abundant elements compared to, for instance, materials made from lanthanides, while also showing less spectral overlap of absorption and emission spectra compared to commercially used inexpensive Lumogen F dyes[56], which are commonly used in LDS layers. In theory, this would make LDS layers made from Ca-exchanged hackmanites potential. However, since the solar spectrum consists of 44.7 % visible (380-780 nm), 6.6 % UV (< 380 nm) and 48.7 % infrared radiation (> 780 nm)[57], technologies based on up-conversion could be more appealing in spectral modification applications, although spectral modification applications are severely falling behind concentrating multijunction photovoltaics in terms of performance.[55]

4.5 Future

To understand yellow and NIR tenebrescence in hackmanites better, the working mechanisms of both properties should be solved. The first step of solving the mechanisms would be carrying out SEM-EDX measurements to obtain the nanometre scale elemental compositions of the materials showing yellow and NIR tenebrescence. Agamah et al.[3] carried out SEM-EDX measurements in solving the elemental structure of natural hackmanites. SEM pictures can also give information of whether various cations and anions have entered the sodalite structure instead of showing as salt impurities outside the sodalite structure in the XRF results. Additionally, SEM pictures of the yellow area of the sample could be compared to non-coloured area of the sample to possibly obtain additional information. Furthermore, XPS measurements of white and yellow areas could give information of the species and their valence states in those areas.[9] The trap depths of the Ca-exchanged hackmanites could also be measured using thermotenebrescence.[8] In addition to already performed tenebrescence excitation measurements, colour bleaching spectra could be measured to see at which wavelengths the yellow or NIR tenebrescence colour can be removed, and, thus, find out the locations of the ground levels of the colour centres.[9] Additionally, to obtain additional information about the impurities and structures of the materials, EPR measurements could be carried out that gave information about structural effects of energy storage to Norrbo et al.[9] Finally, Ca-exchanged hackmanites could be computationally investigated, in addition to performing quantum chemical

calculations to obtain additional information, which ultimately lead to the understanding of the working principle of purple tenebrescence of hackmanites.[21]

Once the working mechanism of yellow and NIR tenebrescence is clearer, improving those properties, for example, with doping or adjusting ratios of different cations could be performed. It would also be interesting to synthesize hackmanites from various starting materials containing calcium to see if it is possible to obtain hackmanites from those starting material and to see if hackmanites made from them have additional properties. Some future challenges considering potential applications have also been presented in section 4.4.

5 Conclusion

Hackmanites have been successfully synthesized using various starting materials as starting materials instead of zeolite A. Furthermore, various cations and anions have been used in synthesizing hackmanites, although further SEM-EDX measurements are required to confirm that the cations and anions have entered the sodalite structure. Finally, various ion-exchange reactions have been performed on zeolite A to see whether it is possible to synthesize hackmanites from the ion-exchanged products.

Synthesized hackmanites show various photoluminescence, PeL and tenebrescence properties. Blue, light blue, purple, yellow and red photoluminescence emission was obtained from different hackmanite products. Blue and light blue emission was obtained by partly exchanging Na cations with either Ca, Li, Mg or Sr cations and under 254/302 nm UV irradiation, while addition of Br also resulted in bright blue emission under 254 nm UV irradiation. Partly exchanging Na cations with Ba cations resulted in yellow emission under 302 nm UV irradiation. Finally, red emission under 302/365 nm UV irradiation was obtained by partly exchanging Na cations with Ca cations. Traditional purple tenebrescence colour after 254 nm UV irradiation was obtained in un-doped products, as well as by partly exchanging Na cations with either K, Mg, Li or Rb.

Yellow and NIR tenebrescence, two completely new properties for hackmanites, were obtained in Ca-exchanged hackmanites. It was suggested that the yellow tenebrescence colour could originate from Ca partly substituting Na in the sodalite structure, resulting in structural changes, and making the formed F-centres absorb higher energy photons at 2.9 eV instead of photons at 2.3 eV. However, no working mechanisms

of yellow or NIR tenebrescence were presented in this work. All things considered, Ca-exchanged hackmanites could have excellent properties and potential to be used as materials in advanced anti-counterfeiting applications.

References

1. Lee, O. I. A new property of matter: Reversible photosensitivity in hackmanite from Bancroft, Ontario. *Am. Mineral.* **21**, 764 (1936).
2. Williams, E. F., Hodgson, W. G. & Brinen, J. S. Synthetic Photochromic Sodalite. *J. Am. Ceram. Soc.* **52**, 139–144 (1969).
3. Agamah, C. *et al.* Hackmanite-the natural glow-in-the-dark material. *Chem. Mater.* **32**, 8895–8905 (2020).
4. Medved, D. B. Hackmanite and Its Tenebrescent Properties. *Am. Miner.* **39**, 615–629 (1954).
5. International Mineralogical Association. List of Minerals (accessed June 1st 2021).
6. Norrbo, I., Gluchowski, P., Paturi, P., Sinkkonen, J. & Lastusaari, M. Persistent Luminescence of Tenebrescent $Na_8Al_6Si_6O_{24}(Cl,S)_2$: Multifunctional Optical Markers. *Inorg. Chem.* **54**, 7717–7724 (2015).
7. Norrbo, I. *et al.* Lanthanide and Heavy Metal Free Long White Persistent Luminescence from Ti Doped Li–Hackmanite: A Versatile, Low-Cost Material. *Adv. Funct. Mater.* **27**, (2017).
8. Norrbo, I. *et al.* Solar UV index and UV dose determination with photochromic hackmanites: From the assessment of the fundamental properties to the device. *Mater. Horizons* **5**, 569–576 (2018).
9. Norrbo, I. *et al.* Mechanisms of Tenebrescence and Persistent Luminescence in Synthetic Hackmanite $Na_8Al_6Si_6O_{24}(Cl,S)_2$. *ACS Appl. Mater. Interfaces* **8**, 11592–11602 (2016).
10. Hassan, I., Antao, S. M. & Parise, J. B. Sodalite: High-temperature structures obtained from synchotron radiation and Rietveld refinements. *Mineral. Mag.* **68**, 499–513 (2004).
11. Hassan, I. & Grundy, H. D. The Crystal Structures of Sodalite-Group Minerals. *Acta Cryst.* **B40**, 6–13 (1984).
12. Medved, D. B. The optical properties of natural and synthetic hackmanite. *J. Chem. Phys.* **21**, 1309–1310 (1953).
13. Williams, E. R., Simmonds, A., Armstrong, J. A. & Weller, M. T. Compositional and structural control of tenebrescence. *J. Mater. Chem.* **20**, 10883–10887 (2010).
14. Zahoransky, T., Friis, H. & Marks, M. A. W. Luminescence and tenebrescence of natural sodalites: a chemical and structural study. *Phys. Chem. Miner.* **43**, 459–480 (2016).
15. Schipper, D. J., Van Doorn, C. Z. & Bolwijn, P. T. Preparation of Cathodochromic Sodalites. **55**, 256–259 (1971).

16. Norrbo, I., Hyppänen, I. & Lastusaari, M. Up-conversion luminescence – A new property in tenebrescent and persistent luminescent hackmanites. *J. Lumin.* **191**, 28–34 (2017).

17. Sidike, A. *et al.* Fine structure in photoluminescence spectrum of S^{2-} center in sodalite. *Phys. Chem. Miner.* **34**, 477–484 (2007).

18. Gaft, M., Panczer, G., Nagli, L. & Yeates, H. Laser-induced time-resolved luminescence of tugtupite, sodalite and hackmanite. *Phys. Chem. Miner.* **36**, 127–141 (2009).

19. Van Doorn, C. Z. & Schipper, D. J. Luminescence of O^{2-}, Mn^{2+} and Fe^{3+} in Sodalite. *Phys. Lett.* **34**, 139–140 (1971).

20. Byron, H., Norrbo, I. & Lastusaari, M. A zeolite-free synthesis of luminescent and photochromic hackmanites. *J. Alloys Compd.* **872**, 159671 (2021).

21. Curutchet, A. & Le Bahers, T. Modeling the Photochromism of S-Doped Sodalites Using DFT, TD-DFT, and SAC-CI Methods. *Inorg. Chem.* **56**, 414–423 (2017).

22. Wang, J., Gao, Y., Zhang, J. & Tian, H. Invisible photochromism and optical anticounterfeiting based on D–A type inverse diarylethene. *J. Mater. Chem. C* **5**, 4571–4577 (2017).

23. Ren, Y. *et al.* Reversible Upconversion Luminescence Modification Based on Photochromism in $BaMgSiO_4$:Yb^{3+},Tb^{3+} Ceramics for Anti-Counterfeiting Applications. *Adv. Opt. Mater.* **7**, 1900213 (2019).

24. Huang, G. *et al.* Multiple Anti-Counterfeiting Guarantees from a Simple Tetraphenylethylene Derivative – High-Contrasted and Multi-State Mechanochromism and Photochromism. *Angew. Chemie* **131**, 17978–17983 (2019).

25. Jiang, K. *et al.* Triple-Mode Emission of Carbon Dots: Applications for Advanced Anti-Counterfeiting. *Angew. Chemie* **128**, 7347–7351 (2016).

26. Xu, L. *et al.* Double-Protected All-Inorganic Perovskite Nanocrystals by Crystalline Matrix and Silica for Triple-Modal Anti-Counterfeiting Codes. *ACS Appl. Mater. Interfaces* **9**, 26556–26564 (2017).

27. Luo, J., Zhang, H. & Yang, J. Hydrothermal Synthesis of Sodalite on Alkali-Activated Coal Fly Ash for Removal of Lead Ions. *Procedia Environ. Sci.* **31**, 605–614 (2016).

28. Carvalho, J. M. *et al.* Fast, low-cost preparation of hackmanite minerals with reversible photochromic behavior using a microwave-assisted structure-conversion method. *Chem. Commun.* **54**, 7326–7329 (2018).

29. Yang, S., Kim, J. & Ahn, W. Microporous and Mesoporous Materials CO_2 adsorption over ion-exchanged zeolite beta with alkali and alkaline earth metal ions. *Microporous Mesoporous Mater.* **135**, 90–94 (2010).

30. Kayiran, S. B. & Darkrim, F. L. Synthesis and ionic exchanges of zeolites for gas adsorption. 100–104 (2002). doi:10.1002/sia.1262

31. Vuori, S. Synthetic hackmanites as detection materials for ionizing radiation. (2019).

32. Rietveld, H. M. A profile refinement method for nuclear and magnetic structures. *J. Appl. Crystallogr.* **2**, 65–71 (1969).

33. Finch, A. A. Conversion of nepheline to sodalite during subsolidus processes in alkaline rocks. *Mineral. Mag.* **55**, 459–463 (1991).

34. Henderson, B., Stokowski, S. E. & Ensign, T. C. Luminescence from F Centers in Calcium Oxide. *Phys. Rev.* **183**, (1969).

35. Cheng, J., Wang, C. F., Zhang, Y., Yang, S. & Chen, S. Zinc ion-doped carbon dots with strong yellow photoluminescence. *RSC Adv.* **6**, 37189–37194 (2016).

36. Wang, L. *et al.* Europium(II)-activated oxonitridosilicate yellow phosphor with excellent quantum efficiency and thermal stability - A robust spectral conversion material for highly efficient and reliable white LEDs. *Phys. Chem. Chem. Phys.* **17**, 15797–15804 (2015).

37. Yasumori, A., Tada, F., Yanagida, S. & Kishi, T. Yellow Photoluminescence Properties of Copper Ion Doped Phase–Separated Glasses in Alkali Borosilicate System. *J. Electrochem. Soc.* **159**, J143–J147 (2012).

38. Gao, C. *et al.* Luminescence enhancement in bromine and samarium co-doped TiO_2 semiconductor nanocrystalline powders. *J. Lumin.* **128**, 559–564 (2008).

39. Ju, G., Hu, Y., Chen, L., Wang, X. & Mu, Z. Blue persistent luminescence in Eu^{2+} doped $Ca_3Mg_3(PO_4)_4$. *Opt. Mater. (Amst).* **36**, 1183–1188 (2014).

40. Finley, E., Cobb, A., Duke, A., Paterson, A. & Brgoch, J. Optimizing Blue Persistent Luminescence in $(Sr_{1-\delta}Ba_\delta)_2MgSi_2O_7:Eu^{2+},Dy^{3+}$ via Solid Solution for Use in Point-of-Care Diagnostics. *ACS Appl. Mater. Interfaces* **8**, 26956–26963 (2016).

41. Li, M., Yu, X., Wang, T., Qiu, J. & Xu, X. White-blue long persistent luminescence in $Ca_2Ge_7O_{16}:Tb^{3+}$ via persistent energy transfer. *Ceram. Int.* **41**, 11523–11527 (2015).

42. Pan, Z., Lu, Y. Y. & Liu, F. Sunlight-activated long-persistent luminescence in the near-infrared from Cr^{3+}-doped zinc gallogermanates. *Nat. Mater.* **11**, 58–63 (2012).

43. Zeng, J. *et al.* In-situ Insights into trap attributions in Fe^{3+}-activated long persistent phosphors. *J. Lumin.* **232**, 117810 (2021).

44. Blumentritt, F. *et al.* Unravelling the Origin of the Yellow-Orange Luminescence in Natural and Synthetic Scapolites. *J. Phys. Chem. Lett.* **11**, 4591–4596 (2020).

45. Yang, Z., Du, J., Martin, L. I. D. J. & Poelman, D. Reversible yellow-gray photochromism in potassium-sodium niobate-based transparent ceramics. *J. Eur. Ceram. Soc.* **41**, 1925–1933 (2021).

46. Li, Z. *et al.* Solvent-dependent and visible light-activated NIR photochromic dithienylethene modified by difluoroboron β-diketonates as fluorescent turn-on pH sensor. *Dye. Pigment.* **162**, 339–347 (2019).

47. Klaue, K., Garmshausen, Y. & Hecht, S. Taking Photochromism beyond Visible : Direct One-Photon NIR Photoswitches Operating in the Biological Window. *Angew. Chemie - Int. Ed.* **57**, 1414–1417 (2018).

48. Schildhammer, D., Fuhrmann, G., Petschnig, L., Schottenberger, H. & Huppertz, H. Synthesis and optical properties of new highly NIR re fl ective inorganic pigments $RE_6Mo_2O_{15}$ (*RE* = Tb , Dy , Ho , Er). *Dye. Pigment.* **140**, 22–28 (2017).

49. Vuori, S. *et al.* Detection of X-Ray Doses with Color-Changing Hackmanites: Mechanism and Application. *Adv. Opt. Mater.* **2100762**, (2021).

50. Andreani, L. C., Bozzola, A., Kowalczewski, P., Liscidini, M. & Redorici, L. Silicon solar cells: Toward the efficiency limits. *Adv. Phys. X* **4**, (2019).

51. Alonso-Alvarez, D., Klampaftis, E., Ross, D. & Richards, B. S. External thermalization of carriers with luminescent down shifting for lower operating solar cell temperature. *IEEE J. Photovoltaics* **4**, 1532–1537 (2014).

52. Hovel, H. J., Hodgson, R. T. & Woodall, J. M. The effect of fluorescent wavelength shifting on solar cell spectral response. *Sol. Energy Mater.* **2**, 19–29 (1979).

53. Assadi, M. K., Bakhoda, S., Saidur, R. & Hanaei, H. Recent progress in perovskite solar cells. *Renew. Sustain. Energy Rev.* **81**, 2812–2822 (2018).

54. Lee, T. D. & Ebong, A. U. A review of thin film solar cell technologies and challenges. *Renew. Sustain. Energy Rev.* **70**, 1286–1297 (2017).

55. Day, J., Senthilarasu, S. & Mallick, T. K. Improving spectral modification for applications in solar cells: A review. *Renew. Energy* **132**, 186–205 (2019).

56. Alonso-Alvarez, D. *et al.* Luminescent down-shifting experiment and modelling with multiple photovoltaic technologies. *Prog. photovoltaics Res. Appl.* **23**, 479–497 (2015).

57. Fu, S. C. *et al.* Bio-inspired cooling technologies and the applications in buildings. *Energy Build.* **225**, (2020).

58. a) Int. Cent. Diffr. Data, PDF-4 + 2018, entry 01-083-4890 (Nepheline)

    b) Swanson, Fuyat. Natl. Bur. Stand. (U. S.), Circ. 539 (1953), II, 41., PDF-4 + 2018, entry 00-005-0628 (NaCl)

    c) Welton, J. and McCarthy, G., North Dakota State Univ., Fargo, ND, USA. ICDD Grant-in-Aid (1989), PDF-4 + 2018, entry 00-041-1476 (KCl)

    d) Liu, G., McMaster Univ., Hamilton, Ontario, Canada; Eick, H., Michigan State Univ., E. Lansing, MI, USA. Private Communication (1994), PDF-4 + 2018, entry 00-045-1313 ($BaCl_2$)

    e) Int. Cent. Diffr. Data, PDF-4 + 2018, entry 01-071-5401 ($CaBr_2$)